Rap1 promotes epithelial integrity and cell viability in a growing tissue

C. Luke Messer and Jocelyn A. McDonald*

Division of Biology, Kansas State University, Manhattan, KS 66506

*Correspondence: jmcdona@ksu.edu

Running Title: Rap1 promotes epithelial integrity and cell survival

Abstract

Having intact epithelial tissues is critical for embryonic development and adult homeostasis. How epithelia respond to damaging insults or tissue growth while still maintaining intercellular connections and barrier integrity during development is poorly understood. The conserved small GTPase Rap1 is critical for establishing cell polarity and regulating cadherin-catenin cell junctions. Here, we identified a new role for Rap1 in maintaining epithelial integrity and tissue shape of a growing tissue, the *Drosophila* egg chamber during oogenesis. Loss of Rap1 activity disrupted the follicle cell epithelium and shape of egg chambers. While Rap1 did not control the localization of non-muscle myosin II (Myo-II), it was required for the apical enrichment of E-Cadherin in some cells. Both Myo-II and the adherens junction-cytoskeletal linker protein α-Catenin were required for normal egg chamber shape. Further, we found that Rap1 promoted epithelial cell survival. Follicle cells deficient for Rap1 had increased caspase activity and underwent apoptosis. Loss of Myo-II did not affect cell survival, though loss of α-Catenin resulted in a mild increase in cells undergoing apoptosis. Blocking the apoptotic cascade failed to rescue the cell shape defects caused by Rap1inhibition. One consequence of increased cell death caused by Rap1 inhibition was the preferential loss of the polar cells, which later in development led to fewer cells forming a properly migrating border cell cluster. Our results thus indicate dual roles for Rap1 in controlling epithelial morphogenesis and cell survival of a growing tissue during development.

Introduction

Epithelial cells form tightly knit sheets that function as coverings and linings for most of the body's surfaces. From the epidermis of the skin to the lining of the gut, epithelia aid in protection from pathogens, immune response, absorption of nutrients, and wound healing (Abramson and Anderson, 2017; Blanpain and Fuchs, 2009; Bröer, 2008; Guillot and Lecuit, 2013; Tai et al., 2019). Epithelial tissues contribute heavily to metazoan growth and development driving dramatic tissue rearrangements during embryogenesis, for example convergent extension in *Drosophila* (Irvine and Wieschaus, 1994), ventral enclosure in *C. elegans* (Williams-Masson et al., 1997), and bottle cell invagination in *Xenopus* (Keller, 1981). The prevalence of epithelial tissues in the animal body plan also makes them vulnerable to diseases like cancer, with epithelial carcinomas accounting for as much as 90% of all human cancers in tissues ranging from breast to colon (Hinck and Näthke, 2014). Work in model organisms has established a foundation of knowledge about characteristics essential for epithelial cells to form functional tissues in vivo. Epithelial cells must establish apicobasal polarity and specialized adhesions between neighboring cells and with the extracellular matrix. Apicobasal polarity is essential for absorption and secretion, ensuring that cargos make it to the appropriate cellular and tissue compartments, while successful cell-cell adhesions allow the transmission of force needed for development and to promote barrier integrity that restricts pathogens (Buckley and St Johnston, 2022; Fernandez-Gonzalez and Peifer, 2022; Rodriguez-Boulan and Macara, 2014).

Epithelial tissues are often challenged by cell turnover and cellular rearrangement in response to normal tissue growth and cell death (Duszyc et al., 2017; Guillot and Lecuit, 2013). How epithelia maintain strong barrier function while being amenable to tissue growth, reorganization, or turnover is a key area of interest in both developmental and disease biology. Epithelia remove, replace, or rearrange cells with little or no tissue disruption. Epithelia can extrude apoptotic cells, for example, by using actomyosin purse-strings that help push the exiting cell out with basal lamellipodia from neighboring cells working to "re-seal" any gaps that would challenge tissue integrity (Kuipers et al., 2014; Le et al., 2021; Rosenblatt et al., 2001). Similarly, epithelia handle complicated cellular rearrangements with little difficulty. During *Drosophila* germband extension lateral cells of the blastoderm epithelium move posteriorly and intercalate lengthening the embryo along the anterior-posterior axis, a process requiring calculated neighbor exchanges and sophisticated manipulation of cell-cell adherens junctions (Paré and Zallen, 2020; Perez-Vale and Peifer, 2020). Despite advances made in the field of epithelial morphogenesis, we know very little about how epithelial cells and tissues respond to organ growth in tissues devoid of proliferation or rearrangement.

Drosophila oogenesis is an excellent model system to investigate how epithelial cells and tissues respond to growth during development. The ovary is composed of approximately 15 ovarioles, which is a string of progressively developing egg chambers that begins with a germarium, housing both germline and somatic stem cells, and ends with a mature fertilized egg. Each egg chamber consists of 15 germline derived nurse cells and a posterior oocyte and is surrounded by a continuous monolayer of somatically-derived follicle cells (Duhart et al., 2017). The apical domain of this follicle cell epithelium faces the germline, while the basal side contacts the collagen-rich basement membrane on the outside.

Follicle cells maintain cell-cell adhesions between one another to collectively form a hexagonal sheet (Cetera and Horne-Badovinac, 2015; Haigo and Bilder, 2011). Follicle cells continue to proliferate until stage 6, giving rise to an entire population of ~650 mature follicle cells (Spradling, 1993). While follicle cells during early to mid-oogenesis are generally similar in identity and are not yet fated, a pair of cells at both the anterior and posterior ends of the egg chamber called polar cells are fully differentiated. Later, the anterior polar cells specify the surrounding follicle cells to become migratory border cells (Deng et al., 2001; Silver and Montell, 2001). During mid-oogenesis, the entire egg chamber rotates (Cetera and Horne-Badovinac, 2015; Uechi and Kuranaga, 2018). The follicle cells migrate as a collective orthogonal to the anterior-posterior axis of the egg chamber, spinning the egg chamber along its axis as the follicle cells secrete proteins that reinforce the nascent basement membrane. The result of this tissue behavior is a polarized basement membrane that coils around the egg chamber like thread on a spool, which helps the egg achieve its final elongated shape (Haigo and Bilder, 2011; Isabella and Horne-Badovinac, 2016; Lerner et al., 2013; Zajac and Horne-Badovinac, 2022).

Between stages 6 and 9, the follicle cell epithelium accommodates a near two-fold increase in egg chamber length driven by the expansion of germline cells. Germline expansion and the follicle cell response is constrained by a collagen-rich basement membrane that is assembled in part by the circumferentially migrating follicle cells. Along the length of the egg chamber, there is a stiffness gradient of the basement membrane, with weaker stiffness and basement membrane accumulation at each pole (Crest et al., 2017; Haigo and Bilder, 2011). This feature, combined with unbiased germline expansion, contributes to the characteristic ovoid shape of the developing egg chamber. In addition to the post-mitotic nature of the tissue at this stage, follicle cell rearrangement is minimal during this period of egg chamber elongation (Alégot et al., 2018; Haigo and Bilder, 2011). Therefore, *Drosophila* oogenesis, particularly the key elongation period between stages 6-9, is an exceptional model to investigate how epithelial

cells and tissues respond to organ growth in the absence of cell division or dramatic cellular rearrangements.

The small GTPase Rap1 is required for epithelial morphogenesis during development, especially in establishing tissue polarity and maintaining adherens junctions. In the *Drosophila* embryo, Rap1 helps polarize epithelial cells by positioning Bazooka/Par3 (Bonello et al., 2018; Choi et al., 2013). In the *Drosophila* pupal wing, Rap1 promotes proper cell-cell adhesion, as *Rap1* mutant cells condense adherens junctions to one side of the cell and these cells lose proper contacts with their neighbors (Knox and Brown, 2002). Similarly, RAP1GAP expressing human podocytes, which have less active GTP-bound Rap1, have decreased integrin activation, and thus disrupted adhesion to basement membrane components (Potla et al., 2014). Rap1 also promotes dynamic cell shape changes during development, including the elongation of cells at the leading edge of the lateral epidermis during *Drosophila* dorsal closure (Boettner and Van Aelst, 2007; Boettner et al., 2003). Given these roles for Rap1 in cell polarity, cell adhesion, and cell shape changes during development of various tissues and organs, we asked if Rap1 is required for tissue integrity during *Drosophila* oogenesis.

Here we show that Rap1, coupled with proper actomyosin contractility communicated through the α-Catenin/E-Cadherin adherens junction, is required for epithelial cell and tissue shape maintenance during a specific period of egg chamber growth. We identified a role for Rap1 and α-Catenin in maintaining epithelial cell survival more generally, along with more specific effects of Rap1 on the organizing polar cells. Finally, we found that later in oogenesis the pro-survival function of Rap1 in polar cells is critical for producing migratory border cell clusters of the correct size.

Results

Rap1 GTPase is required for proper egg chamber shape in mid-oogenesis

To better understand the roles of Rap1 during oogenesis, we first analyzed the localization of Rap1 using a functional GFP-Rap1 fusion protein expressed under the control of the endogenous *Rap1* promoter (Knox and Brown, 2002). Rap1 is expressed ubiquitously in all cells, with highest enrichment at the apical cell cortex of follicle cells, including the polar cells (Fig. 1A). Rap1 has known roles in the morphogenesis of diverse epithelia (Kim et al., 2022; Knox and Brown, 2002; Wang et al., 2013). Therefore, we wanted to determine if and how Rap1 contributes to the organization of the follicular epithelium. We inhibited Rap1 activity in the follicle cells using a validated dominant negative Rap1 construct, UAS-DN-Rap1^{N17}(Boettner et al., 2003; Sawant et al., 2018), driven by an epithelial-specific GAL4 driver, *c306*-GAL4 (Fig.

1B). While expression of *c306*-GAL4 begins early during oogenesis in anterior and posterior follicle cells, the highest expression occurs at mid-oogenesis (~stages 4-8). These stages coincide with a dramatic anisotropic growth of the egg chamber from a round to ovoid shape (Crest et al., 2017; Haigo and Bilder, 2011; Spradling 1993). This allowed us to test if Rap1 was required during this critical growth phase of the tissue.

The shape of egg chambers at stages 4-to-6 appeared normal in both control and DN-Rap1^{N17} egg chambers (Fig. 1C-D). However, by stages 7-8, DN-Rap1^{N17}-expressing egg chambers no longer had a normal shape (Fig. 1D). The anterior end of DN-Rap1^{N17} egg chambers was wider and flatter compared to control (Fig. 1C-D). Closer inspection of these egg chambers revealed altered anterior epithelial follicle cell shapes specifically in the *c306*-GAL4 expression region (Fig. 1B, D). DN-Rap1^{N17} follicle cells appeared to be stretched, rather than the expected cuboidal follicle cell shapes in control egg chambers at these stages (Fig. 1E-F). We further quantified the observed differences in anterior egg chamber shape, which we termed "local deformation". To do this, we measured the width of the anterior egg chamber at 20% of the total egg chamber length from the anterior end (*see* Materials and Methods). Control egg chambers retained a characteristic "wedge" shape in this anterior region (mean of 37.49µm). DN-Rap1^{N17} inhibited egg chambers, however, were wider and more "cup" shaped (mean of 47.37µm; Fig. 1G). These data together suggest that Rap1 promotes tissue shape, likely through regulation of epithelial morphogenesis.

Rap1 promotes polar cell shape and apical E-Cadherin accumulation

In addition to the overall distorted anterior follicular epithelial cell shapes in DN-Rap1^{N17} egg chambers, we observed particularly misshapen anterior polar cells compared to control (Fig. 1E-F; 2A-B). Polar cells are a specialized pair of follicle cells found at each pole of the egg chamber. Polar cells are one of the first specified follicle cells in the ovary and express unique cell markers such as the adhesion protein Fasciclin III (Fas III) (Ruohola et al., 1991). Because anterior egg chamber shape was most impacted by Rap1 inhibition, we focused on the anterior polar cells. We asked when and how polar cell shape was altered by loss of Rap1 activity. To do this, we quantified anterior polar cell shapes by defining their aspect ratio (AR). We measured the width of each polar cell along their dorsoventral (DV) axis and divided by their length along the anterior-posterior (AP) axis (Fig. 2C). Control polar cells at stages 4-6 were typically longer along the AP axis than they were wide along the DV axis (AR=0.61; Fig. 2A, A', C). At stages 4-6, DN-Rap1^{N17} polar cell shape resembled control (AR=0.65; Fig. 2B, B', C). Control polar cells

maintained their earlier ellipsoid shape at stages 7-8, although they lengthened slightly along the AP axis (AR=0.56; Fig. 2A, A", C). In contrast, Rap1 inhibited polar cells at stage 7/8 frequently lost this elliptical shape and were now extended along the DV axis, with more spherical shapes (AR=1.02; Fig. 2B, B", C). Rap1-inhibited egg chambers also had more extreme cases of abnormal polar cell morphology, with either one polar cell that appeared to be missing (Fig. S1A) or a distortion of the polar cell pair, such as pulling apart into "dumbbell" type shapes (Fig. S1B).

The defective polar cell shapes combined with examples that appeared to split apart prompted us to ask if polar cells in DN-Rap1^{N17} egg chambers were less adhesive. The homophilic cell-cell adhesion protein E-Cadherin accumulates at high levels in polar cells (Niewiadomska et al., 1999). E-Cadherin, as well as the associated cadherin-catenin complex member β-Catenin, highly localizes to the apical side of polar cells, particularly in the region where the polar cell pair is apically constricted (Niewiadomska et al., 1999; Peifer et al., 1993). Therefore, we next investigated if DN-Rap1^{N17} egg chambers accumulated E-Cadherin normally in polar cells (Fig. 3). We measured the apical E-Cadherin fluorescence intensity in stage 7-8 egg chambers along a line drawn starting over the anterior-most nurse cell ("1"; Fig. 3A', B') that extended through the apical polar cell-polar cell interface to the lateral interface ("2"; Fig. 3A', B', C). In control egg chambers, we observed an intense spike of fluorescence signal as the line passed through the apical polar cell-polar cell interface (Fig. 3A-A", C, D). Strikingly, in DN-Rap1^{N17} egg chambers the apical fluorescence enrichment is severely decreased and resembled the intensity values for the portion of the line that extended along the lateral interface (Fig. 3B-B", C, D). These results indicate that Rap1 controls the localized enrichment of E-Cadherin to the apical interface between polar cells, which in turn likely promotes the normal shape of the polar cell pair.

Non-muscle myosin II (Myo-II), as visualized with a functionally-tagged regulatory light chain, Spaghetti Squash-GFP, Sqh::GFP (Royou et al., 2004), is enriched across the entire apical surface of the anterior polar cell pair as well as other follicle cells (Fig. S2A-A''). However, we did not observe any obvious visual differences in the accumulation of Sqh:GFP at the apical surface of DN-Rap1^{N17} polar cells (Fig. S2B-B"). To confirm this, we quantified Sqh::GFP accumulation by drawing a line across the apical surface of the polar cell pair. We then plotted profiles of the fluorescent intensity values from at least 8 polar cell pairs per genotype. These data indicated no major differences in the Myo-II levels or patterns between control and DN-Rap1^{N17} polar cells (Fig. S2C). Together, our results indicate that Rap1 is dispensable for

accumulation of Myo-II but is required for E-Cadherin apical enrichment in polar cells at mid-oogenesis.

Myo-II and α-Catenin are required for egg chamber morphogenesis

Actomyosin contractility and adhesion both contribute to the shape and integrity of various tissues and organs during development (Harris and Tepass, 2010; Munjal and Lecuit, 2014). Therefore, we wanted to assess whether actomyosin contractility was required for local tissue morphogenesis (Fig. 4A-E). We targeted the Myo-II regulatory light chain with RNAi-mediated knockdown (Sqh RNAi) and measured local deformation. Staged 7-8 egg chambers deficient for Myo-II closely resembled the DN-Rap1^{N17} inhibited egg chambers, with a wider and flatter anterior tissue shape (compare Fig. 4B, E to Fig. 1F, G) These results were unexpected given that Rap1 inhibition did not affect apical Myo-II accumulation, at least in polar cells. Therefore, we reasoned that Rap1 may couple actomyosin contractility to the adherens junctions in the anterior epithelium, as has been described in other tissues (Sawyer et al., 2009).

To test this hypothesis, we next performed RNAi knockdown of E-Cadherin and α-Catenin, members of the adherens junction complex. Surprisingly, E-Cadherin had no effect on egg chamber morphogenesis. Anterior width measurements were no different in E-Cadherin deficient egg chambers when compared to GFP RNAi controls (Fig. 4A, C, E). However, N-cadherin is expressed during these stages and has been shown to undergo compensatory upregulation due to loss of E-Cadherin (Loyer et al., 2015). Thus, we next knocked down α-Catenin (α-Cat), the linker protein that connects cadherin complex members to the cellular F-actin cytoskeleton (Wang et al., 2022; Yonemura et al., 2010). Indeed, downregulation of α-Catenin by RNAi resulted in a wider anterior egg chamber, resembling the tissue shape defects observed with Sqh RNAi and inhibition of Rap1 activity (Fig. 4B, D-E; Fig. 1F-G). Thus, adhesion and actomyosin are required to maintain tissue shapes at mid-oogenesis stages.

We next examined the shape of epithelial follicle cells at the anterior end of the egg chamber when Myo-II or α-Catenin were knocked down (Fig. 4F-I'). Close inspection revealed odd individual cell shapes resembling DN-Rap1^{N17} egg chambers only for α-Catenin RNAi (Fig. 4 H-I') but not Sqh RNAi (Fig. 4G, G'). Notably, we observed a mix of "stretched" or "flattened" follicle cells in α-Catenin RNAi egg chambers along the lateral sides of the egg chamber that looked like the cells in the anterior region of DN-Rap1^{N17} egg chambers (Fig. 4H-I'; compare to Fig. 1F). In the most-affected α-Catenin RNAi egg chambers (Fig. 4I, I'), clumping of cells was observed at the most anterior end closely resembling the cell shapes reported for *α-Catenin* null mutant follicle cells (Sarpal et al., 2012). The similarities in the tissue and epithelial cell shape

phenotypes caused by loss of α-Catenin and Rap1 activity suggest that Rap1 modulates α-Catenin-containing adherens junctions, similar to what was observed during dorsal fold formation in the *Drosophila* embryo (Wang et al., 2013).

Rap1 promotes follicle cell viability

Our analysis of DN-Rap1^{N17} egg chambers at stages 7-8 revealed not only cases of extremely distorted polar cells, but also examples where one polar cell was missing from the required pair (Fig. S1A). These data suggested that Rap1 controls cell survival. Therefore, we analyzed a marker of apoptosis during oogenesis of control and Rap1 mutant ovaries. We stained egg chambers for antibodies to cleaved death caspase-1 (cDcp-1), which recognizes both *Drosophila* effector caspases, Death caspase-1 (Dcp-1) and Death related ICE-like caspase (Drice) (Li et al., 2019). During early oogenesis, excess polar cells ("supernumerary" polar cells) and excess stalk cells form but are eliminated by apoptosis during stages 3-6, whereas in healthy ovarioles other follicle cells do not undergo cell death (Borensztejn et al., 2013; Borensztejn et al., 2018; Khammari et al., 2011; Lebo and McCall, 2021; cDCp-1+ cells; Fig. 5A). However, in DN-Rap1^{N17} ovarioles, in addition to the normal pattern of early polar cell and stalk cell apoptosis, we observed additional later caspase activity in follicle cells during stages 2 through 8 of oogenesis (cDCp-1+ cells; Fig. 5B). We further quantified the number of cDcp-1 cells in control and DN-Rap1^{N17} ovarioles and only saw an increase in apoptotic cells when Rap1 activity was inhibited (Fig. 5C). Activation of Rap1, through expression of constitutively active CA-Rap1^{V12} did not decrease apoptotic cells during oogenesis (Fig. 5C). These data suggest that Rap1 is required for follicle cell survival during oogenesis but is not sufficient to block normal developmental apoptosis.

Because Rap1 promotes both follicle cell survival during oogenesis and epithelial and tissue morphogenesis, we next asked if Myo-II or α-Catenin were similarly required. We analyzed cell death during oogenesis using cDcp-1 in Sqh RNAi, α-Catenin RNAi, and matched control (GFP RNAi) ovarioles. We observed minimal cell death in Sqh RNAi and GFP RNAi controls (Fig. 5D, E, G). However, there was a significant increase in cDcp-1 positive cells for α-Catenin RNAi ovarioles (Fig. 5F, G). These results suggest that while both Myo-II and α-Catenin regulate egg chamber morphogenesis, only α-Catenin is required for viability of the follicle cells. Notably, although α-Catenin RNAi results in an increase in cDcp-1 positive cells, fewer cells per ovariole were cDcp-1 positive than when Rap1 was inhibited (2.6 cDcp-1-positive cells for α-Catenin RNAi, Fig. 5G, compared to 8.8 cDcp-1-positive cells per ovariole for DN-Rap1^{N17}, Fig.

5C). Although these findings suggest that cell adhesion via α-Catenin is required for cell viability, Rap1 may have a greater role in promoting cell survival.

Rap1 promotes polar cell survival by suppressing apoptosis, but polar cell shape defects are not apoptosis-dependent

As described above, loss of Rap1 activity causes loss of follicle cells and polar cells (Fig. 5B-C; Fig. S1A) in addition to defects in polar cell shape (Fig. 2B-C; Fig. S1B). Therefore, we wanted to determine if Rap1 was required to manage elimination of supernumerary polar cells that form at each pole of early egg chambers (Besse and Pret, 2003; Borensztejn et al., 2013; Khammari et al., 2011). Removal of the extra polar cells by apoptosis ensures that only two “mature” polar cells remain at anterior and posterior egg chamber poles by stages 5/6 (Besse and Pret, 2003; Borensztejn et al., 2013; Khammari et al., 2011). One possibility for the absence of polar cells in later staged DN-Rap1^{N17} egg chambers could be a requirement for Rap1 in early polar cell development and elimination. Alternatively, Rap1 could promote the survival of mature polar cells later in oogenesis after these cells are specified.

We first asked if the early specification, development, and elimination of supernumerary polar cells was normal in the absence of Rap1 activity. To address this question, we examined anterior and posterior polar cells in egg chambers from stages 3-10 of oogenesis using Eyes Absent (Eya) and FasIII (Fig. S3A). Eya suppresses polar cell fate and is present in all follicle cells except polar cells (Bai and Montell, 2002) and FasIII specifically marks the polar cell pair (Ruohola et al., 1991). We observed similar numbers of supernumerary polar cells at early stages of development (e.g., stages 3-4 and stages 5-6) in control and DN-Rap1^{N17} (Fig. S3A). Using CA-Rap1^{V12}, we next asked if increased Rap1 activity resulted in extra polar cells being maintained until maturity (Boettner et al., 2003; Sawant et al., 2018). At each stage examined, we observed similar numbers of polar cells for CA-Rap1^{V12} and controls (Fig. S3A). Moreover, in all genotypes, in agreement with other studies, there was an overall decrease in the number of polar cells as oogenesis progressed (Fig. S3A; Borensztejn et al., 2013; Khammari et al., 2011).

Since early polar cell development appeared normal in Rap1-deficient egg chambers, we next asked if Rap1 regulated the survival of mature polar cells later in oogenesis. We tracked polar cell-specific accumulation of cDcp-1. Control “mature” polar cells at stages 7-8 rarely died (Fig. 6A-A”;1 out of 66 egg chambers). In contrast, we observed an increased frequency in the accumulation of cDcp-1 in staged 7-8 DN-Rap1^{N17} polar cells, well after the conclusion of normal developmental apoptosis (Fig. 6B-B”; 7 out of 61 egg chambers). These polar cells were frequently pyknotic as visualized by DAPI staining (Fig. 6B’). These data

together indicate that Rap1 promotes the survival of both follicle cells and mature polar cells during later stages of oogenesis.

To further characterize this increase in polar cell death when Rap1 was inhibited, we next examined the apoptotic cascade. Death-associated inhibitor of apoptosis 1 (DIAP1) blocks caspase activity and thus prevents cells from undergoing apoptosis (Hay et al., 1995; Yan et al., 2004). DIAP1 specifically accumulates in the two mature polar cells and promotes their survival, whereas DIAP1 is downregulated in the supernumerary polar cells leading to their developmental apoptosis (Borensztejn et al., 2013; Khammari et al., 2011). We reasoned that a decrease in DIAP1 might precede the death of mature polar cells observed in DN-Rap1^{N17} egg chambers. Therefore, we analyzed DIAP1 accumulation in polar cells relative to their most adjacent follicle cell neighbors at both stages 4 to 6 and at stages 7 to 8. At the earlier stages (stages 4-6), we observed normal accumulation of DIAP1 in 13 out of 14 control polar cells (Fig. 6C-C”). However, DIAP1 accumulated in only 6 out of 23 DN-Rap1^{N17} polar cells (Fig. 6E-E”). Similarly, at later stages, DIAP1 accumulation was lower in DN-Rap1^{N17} inhibited polar cells, with only 8 out of 19 egg chambers having normal DIAP1 accumulation (Fig. 6F-F”), compared to 10 out of 14 for control egg chambers (Fig. 6D-D”)). Interestingly, DIAP1 levels were altered at a greater frequency in DN-Rap1^{N17} egg chambers (Fig. 6E-F”) than the observed frequency of polar cell death (Fig. 6B”). One possibility is that not all cells that lose DIAP1 accumulation undergo cell death. Alternatively, the threshold for DIAP1 protein depletion must be relatively severe for apoptosis to occur. Taken together, our results favor a role for Rap1 in suppressing the apoptotic cascade through regulating the levels of DIAP1 in mature polar cells.

We next asked if the polar cell morphology defects caused by loss of Rap1 activity were due to apoptosis. To test this, we asked if blocking the apoptotic cascade could rescue polar cell shape defects caused by loss of Rap1 activity (Fig. S3B-D). We performed polar cell aspect ratio measurements in egg chambers that co-expressed DN-Rap1^{N17} with a either LacZ control or with the apoptosis inhibitor, baculoviral p35 (Clem et al., 1991; Hay et al., 1994). We found that co-expression of p35 along with DN-Rap1^{N17} failed to rescue the polar cell aspect ratio defects compared to co-expression with LacZ (Fig. S3B-D). There was no statistical difference in the aspect ratios of DN-Rap1^{N17} polar cells also expressing the LacZ control or p35 (AR=0.84, DN-Rap1^{N17} + LacZ; AR=0.85, DN-Rap1^{N17} + p35; Fig. S3D). These results provide further evidence that Rap1 likely controls polar cell morphogenesis independently of its function in cell survival.

Rap1 requirement for polar cell survival supports formation of border cell clusters with optimal cell numbers

During late stage 8, the anterior pair of polar cells specifies which follicle cell neighbors will become migratory border cells through the secretion of the JAK/STAT ligand, Unpaired (Beccari et al., 2002; Silver and Montell, 2001). Anywhere between 4-8 follicle cells activate high levels of JAK/STAT and subsequently surround the polar cells to produce a border cell cluster with a total number of 6 to 10 cells (Silver and Montell, 2001). Because inhibition of Rap1 caused a frequent loss of mature polar cells, we next determined how this impacts the size of migratory border cell clusters during later oogenesis. We reasoned that losing a polar cell might decrease the number of cells found in border cell clusters. We quantified the total number of cells found within control (UAS-LacZ) versus Rap1-deficient (UAS-Rap1 RNAi or UAS-Rap1^{N17}) border cell clusters (Fig. 7 A-C). When Rap1 was inhibited using either *Rap1* RNAi or DN-Rap1^{N17} driven by *c306*-GAL4, we found a strong reduction in the average number of cells per cluster compared to control (Fig. 7A', B'; average of 6.1 cells in control compared to 4.6 cells in DN-Rap1^{N17}). *c306*-GAL4-driven *Rap1* RNAi also reduced the number of cells per cluster to an average of 5.2 cells compared to 6.1 cells in *mCherry* RNAi controls (Fig. 7C). We also analyzed the number of cells in border cell clusters using a different GAL4, *slbo*-GAL4, which is expressed later than *c306*-GAL4 and in a more restricted pattern (Fig. S4A). The overall number of cells in *slbo*-GAL4 control egg chambers is higher than observed for *c306*-GAL4 controls (average 8.2 cells; Fig. S4B, B', D). Nonetheless, we observed a significant reduction in the number of DN-Rap1^{N17} cells within the border cell cluster (Fig. S4C-D; average 6.7 cells). Thus, Rap1 is required for migrating border cell clusters to have an optimal number of cells.

We next asked if the observed reduction in cell numbers within the border cell cluster was due to Rap1 function in border cell specification or in the recruitment of cells due to cell survival. We examined anterior follicle cells at stage 8 for a reporter of JAK/STAT activity, 10XSTAT::GFP (Bach et al., 2007). These cells are fated to become the migratory border cells (Beccari et al., 2002; Silver and Montell, 2001). We asked if Rap1 inhibition caused changes in JAK/STAT activity in the three follicle cells immediately adjacent to the polar cells at stages 7-8. We were unable to detect any changes in either the pattern of 10XSTAT:GFP or the nuclear STAT levels, and hence activity, when both polar cells were present in DN-Rap1^{N17} compared to control (Fig. S5A-C). These results suggest that border cell fate specification at stage 8 of oogenesis is normal under conditions where both polar cells are present and does not rely on Rap1 activity. However, we cannot rule out a subtle decrease in the JAK/STAT activity gradient when only one polar cell survives to stage 8 in DN-Rap1^{N17} egg chambers.

Finally, we determined if the smaller number of cells per border cell cluster was due to the increase in apoptotic cells observed upon Rap1 inhibition. We co-expressed DN-Rap1^{N17} with either a UAS-LacZ control or the apoptosis inhibitor p35 (Fig. 7D-F). We quantified the number of cells per cluster at stages 9 and 10, when border cell clusters have already formed and normally have either begun to migrate or have finished their migration. Border cell clusters co-expressing DN-Rap1^{N17} and LacZ had an average of 4.8 cells per cluster, closely resembling the phenotypes observed when expressing DN-Rap1^{N17} alone (Fig. 7D, D', F compared to Fig. 7C). In contrast, border cell clusters co-expressing DN-Rap1^{N17} and p35 had an average of 6.4 cells per cluster (Fig. 7E-F), closely resembling control border cell clusters (Fig. 7A, A', C). Given that loss of Rap1 activity causes apoptotic cell death of mature polar cells just prior to recruitment of border cells, we think this likely causes the observed smaller border cell clusters. These data together support our hypothesis that Rap1 promotes mature polar cell survival by preventing apoptosis through upregulation of DIAP1, thus contributing directly to having an optimal number of cells within the migrating border cell cluster.

Discussion

A key challenge in developmental biology is understanding how cells and tissues respond to morphogenesis and growth. The cellular characteristics required for epithelial integrity in the face of dramatic changes in tissue shape and size during normal development remain poorly understood. Here we focused on understanding how the small GTPase Rap1 maintains cell and tissue shapes during *Drosophila* egg chamber elongation. Prior work has shown requirements for Rap1 in epithelial morphogenesis during development, but how this function is coordinated remains unclear (Asha et al., 1999; Boettner and Van Aelst, 2007; Choi et al., 2013; Bonello et al., 2018). Here we used a model of developmental tissue growth to interrogate the function of Rap1 in epithelial integrity. We found that Rap1 maintains individual follicle cell shapes as well as localized tissue shapes during growth of the *Drosophila* ovary. We presented evidence that Rap1 maintains tissue integrity, which we propose is through regulation of dynamic linkages between adherens junctions and the contractile actomyosin cytoskeleton. Our experiments revealed a new role for Rap1 in regulating cell viability, including the mature polar cells, during oogenesis leading to the successful assembly of the migratory border cell cluster.

Rap1 maintains cell and tissue shapes by modulating adherens junction-cytoskeleton linkages during tissue growth

Here we report that Rap1 is required to maintain polar cell and follicle cell shapes and proper tissue shapes of the anterior follicular epithelium during egg chamber elongation. *Rap1* null flies that were rescued to viable adults by expression of heat shock-driven Rap1 revealed egg chambers that degenerated and had distorted follicle cell shapes (Asha et al., 1999). Notably, these phenotypes seemed to be more severe during mid-to-late stages of oogenesis, stages that overlap with egg chamber elongation. We obtained similar, albeit less severe egg chamber degeneration defects, by expressing the DN-Rap1^{N17} specifically in follicle cells. Our quantitative analyses of individual cell shapes and local tissue deformation revealed a major role for Rap1 in maintenance of tissue morphology. Moreover, Rap1-deficient polar cell shapes were most affected by stages 7-8, a period of dramatic egg chamber growth (Crest et al., 2017). These results indicate a requirement of Rap1 in tissue shape maintenance during egg chamber elongation.

How does Rap1 contribute to cell and tissue shape maintenance within the follicular epithelium during tissue expansion? Rap1 regulates early Bazooka/Par3 localization and adherens junction positioning during *Drosophila* embryogenesis (Bonello et al., 2018). *Rap1* mutant embryos fail to localize spot adherens junctions properly during cellularization and complete embryogenesis with fragmented cuticles suggesting a loss of tissue integrity (Choi et al., 2013). Similarly, Rap family proteins are required for adherens junctions and tight junction formation in MDCK cells (Sasaki et al., 2020). Our results show that Rap1 is required specifically for the enrichment of E-Cadherin at the apical side of polar cells. We also observed stretching of the anterior epithelial follicle cells, which could indicate altered adherens junction maintenance. However, E-cadherin appeared to be localized to apical puncta between follicle cells. Moreover, E-Cadherin was not completely lost in polar cells due to Rap1 inhibition. We thus hypothesize that Rap1 maintains (or helps assemble) the proper positioning of the apical adherens junction, at least in polar cells.

The functions of adherens junctions to maintain cell-to-cell contacts within an epithelium are also coupled to actomyosin contractility, which can drive cell shape changes. Rap1 and its effector Canoe (Cno) regulate actomyosin contractility in apically constricting mesodermal cells during *Drosophila* ventral furrow invagination (Sawyer et al., 2009; Spahn et al., 2012). Similarly, Rap1 is required for Shroom dependent apical constriction in *Xenopus* (Haigo et al., 2003). These studies led us to ask if, in addition to its role in positioning adherens junctions during egg chamber elongation, Rap1 was responsible for proper actomyosin contractility. We found that Myo-II was required for proper tissue shape during egg chamber elongation, but surprisingly Rap1 was dispensable for Myo-II localization in polar cells. Taken together with the

stretched individual cell shapes and deformed egg chambers observed for α-Catenin RNAi, these data support our model that Rap1 maintains the strength of adherens junction-actin linkages as was reported for the known Rap1 effector Cno (Sawyer et al., 2009).

We found that Rap1 regulates egg chamber shape during tissue growth. The inherent on-off activity states of GTPases like Rap1 make them particularly useful for dynamic processes that require discrete bursts of activity in response to cellular or tissue level cues (Gloerich and Bos, 2011). In apical constriction, for example, myosin pulsatility is coupled to progressive tightening of the apical domain (Martin and Goldstein, 2014; Martin et al., 2009). The transient nature of pulsatile myosin may require a fast-acting molecular switch that can be activated and inactivated quickly to couple motor behaviors to changes at the cell cortex. While we did not observe Myo-II localization defects when Rap1 was inhibited, the requirement for α-Catenin indicates that linkage to the actomyosin cytoskeleton is critical for epithelial cell and tissue shapes. Atypical Protein Kinase C (aPKC) promotes an optimal level of actomyosin to maintain an intact and organized follicle cell epithelium (Osswald et al., 2022). Indeed, acute loss of aPKC causes the follicle cell layer to apically constrict and rupture, due to growth of the egg chamber. While the effects caused by loss of Rap1 activity did not cause the epithelium to rupture, the tissue instead locally deformed. The basement membrane becomes thinner at the anterior and posterior ends during tissue elongation, allowing further growth along the anterior-posterior axis (Balaji et al., 2019; Crest et al., 2017). We suggest that loss of Rap1 causes the tissue to widen due to the normal reduction in basement membrane during egg chamber growth. Thus, we propose that Rap1, through apical enrichment of the adherens junction, reinforces strong epithelial connections and resistance to growth of the germline.

Rap1 promotes follicle cell and polar cell survival during oogenesis

Our results showed that Rap1 maintains follicle cell and polar cell viability throughout oogenesis. Both Rap1 inhibition and α-Catenin RNAi resulted in an increase in apoptotic cells. One possibility is that the role for Rap1 in E-Cadherin localization is coupled to cell survival. Cell-cell contacts are essential for cell viability in certain contexts (Guillot and Lecuit, 2013). Since the adherens junction-cytoskeleton linker α-Catenin also supports proper adhesion and α-Catenin RNAi resulted in increased caspase activity during oogenesis, this may indicate a role for cell-cell adhesions in cell viability during tissue growth during *Drosophila* oogenesis. This period of dramatic tissue growth likely places extra strain on the epithelial follicle cells (Osswald et al., 2022). Thus, having proper cell-cell adhesions is critical for epithelial integrity and cell survival during tissue morphogenesis.

Rap1 may have independent functions in cell survival other than regulation of adherens junction proteins. Although knocking down α-Catenin resulted in apoptotic cells, the phenotype was overall milder than that observed with Rap1 inhibition. Moreover, we observed a decrease in DIAP1 accumulation in polar cells upon Rap1 inhibition. Rap1 is known to negatively regulate the Hippo (Hpo) pathway in *Drosophila* border cells (Chang et al., 2018). Hippo limits *diap1* transcription by inhibiting downstream transcription factor Yorkie (Yki) (Huang et al., 2005; Wu et al., 2003). Therefore, one possibility is that Rap1 promotes cell viability, especially of the polar cells, by limiting Hpo activity to ensure proper DIAP1 levels. However, additional work will be needed to test this hypothesis. Indeed, we do not yet have a clear understanding of how apoptosis is regulated in this tissue. During stages 7 to 8, egg chambers reduce the overall levels of DIAP1, which serves as a checkpoint mechanism to terminate unhealthy egg chambers rather than commit additional nutritional and energy resources (Baum et al., 2007). Open questions include whether Rap1 generally maintains cell survival of follicle cells by fine tuning DIAP1 or if the regulation of DIAP1 by Rap1 is more indirect, for example due to disruption of epithelial integrity when Rap1 is inhibited. It is also unclear how cellular mechanics function together with transcription of DIAP1 to promote cell viability.

The signal relay mechanisms that act upstream to regulate the various Rap1 activities in the follicle cell epithelium are unknown. Nor is it known which Rap1 effectors mediate the direct control of adherens junction-actomyosin linkages in this context. The GTPase activating protein Rapgap1 acts as one regulatory layer controlling Rap1 α-Catenin modulation in regulating dorsal fold morphogenesis and is expressed in the ovary (Wang et al., 2013; Sawant et al., 2018). *Drosophila* has several known guanine nucleotide exchange factors (GEFs), including PDZ-GEF (also known as Dizzy). Whether one or more GEFs have differential functions during oogenesis remains to be tested. A well-known Rap1 effector, Cno, acts as a key signal relay mechanism downstream of Rap1. For example Cno mediates Rap1 functions in *Drosophila* morphogenesis including mesoderm invagination, head involution, and dorsal closure through modular biochemical functions (Sawyer et al., 2009; Perez-Vale et al., 2021). Further experiments will be required to identify if these or other upstream and downstream regulators mediate Rap1 functions in the ovary and if these roles are conserved.

MATERIALS AND METHODS

Drosophila genetics

All fly stocks used in this study are listed in Table 1 and the complete genotypes for each experiment can be found in Table 2. Crosses were typically set up and maintained at 25˚C. In cases where transgene expression impacted organism viability, the crosses were set up and maintained at 18˚C. The tub-GAL80ts ('tsGAL80') transgene (McGuire et al., 2004) was present in the genetic background of many crosses in this study to repress GAL4 expression during other stages of development. Flies were shifted to 29˚C for 12-72 hours prior to dissection to ensure optimal GAL4 expression and repression of tsGAL80, unless otherwise noted.

Immunostaining

Antibodies, sources, and dilutions used are listed in Table 3. Fly ovaries from 2- to 8-day old females were dissected in Schneider's *Drosophila* Medium (Thermo Fisher Scientific, Waltham, MA, USA) supplemented with 10% fetal bovine serum (Seradigm FBS; VWR, Radnor, PA, USA). Ovaries were either kept whole or dissected further into ovarioles and fixed for 10 mins using 16% methanol-free formaldehyde (Polysciences, Inc., Warrington, PA, USA) diluted to a final concentration of 4% in 1X Phosphate Buffered Saline (PBS). Following fixation, tissues were washed ≥4x with 'NP40 block' (50 mM Tris-HCL, pH 7.4, 150mM NaCl, 0.5% NP40, 5mg/ml bovine serum albumin [BSA]) and rocked in the solution for ≥30 mins prior to antibody incubation. Primary and secondary antibody incubation as well as all other subsequent wash steps were also performed in NP40 block. Dissected and stained ovarioles and egg chambers were mounted on slides with Aqua-PolyMount (Polysciences, Inc.) media and allowed to harden prior to imaging.

Microscopy

Images of fixed egg chambers were acquired on a Zeiss LSM 880 confocal laser scanning microscope (KSU College of Veterinary Medicine Confocal Core) using either a 20 X 0.75 numerical aperture (NA) or a 40 X 1.3 NA oil-immersion objective controlled by Zeiss Zen 14 software.

Image Processing and Data Analysis

Measurements were performed using FIJI (Schindelin et al., 2012). Egg chamber local deformation measurements were determined by measuring the width between the apical follicle cell surfaces at 20% of the anterior-posterior (A-P) length of the egg chamber (the very anterior tip is 0% of the A-P length). The polar cell aspect ratio was measured by analyzing Z-stacks taken of egg chambers stained with FasIII (to identify polar cells), E-Cadherin, and DAPI; the

length and width was measured at the widest point of each polar cell. The aspect ratio was then calculated by dividing the width by length.

E-Cadherin accumulation in polar cells (identified by FasIII) was measured by analyzing Z-stacks acquired of egg chambers stained for E-Cadherin, FasIII, and DAPI. A 7µm line was drawn to quantify pixel intensity, starting within the germline (an adjacent nurse cell), extending through the apical polar cell-polar cell contact, then continuing along the lateral interface (see line in Fig. 3A' and 3B'). Only images in which both polar cells could be viewed in the same Z-slice were used for quantitation. The "Plot Profile" function in FIJI was used to obtain a list of pixel intensity values corresponding to points along this line. These values were normalized to the highest pixel intensity measured in the experiment and plotted. Staining and imaging conditions were kept consistent between samples.

Dying cells during oogenesis were quantified by scanning through dissected whole ovarioles stained and imaged for cDcp-1, DAPI, and FasIII. Nuclei positive for caspase activity (cDcp-1-expressing nuclei) from stages 2 through 8 were quantified. Death of mature polar was scored by analyzing cDcp-1 expressing nuclei specifically in stage 7-8 egg chambers. DIAP1 accumulation in polar cells was assessed by acquiring Z-stacks through the polar cells in stages 4-6 and stages 7-8 egg chambers and analyzing qualitative reduction in the DIAP1 signal compared to adjacent cells. Polar cells were identified using a GFP protein trap in FasIII.

Quantification of the number of cells per border cell cluster were measured by acquiring Z-stacks through border cell clusters visualized using the nuclear envelope marker Lamin (also known as Lamin Dm_0) and DAPI. Whenever possible, E-Cadherin was used to determine the boundaries of fully delaminated border cell clusters. Z-stacks encompassing the entire cluster including both border cells and polar cells were acquired and nuclei were manually counted using the Lamin signal.

Apical Myo-II accumulation was quantified by acquiring Z-stacks of stage 7-8 egg chambers expressing a fluorescent Myo-II reporter, Sqh::GFP, and co-stained for E-Cadherin and DAPI. A 2µm line was drawn at the apical surface of polar cells (identified by enrichment of E-Cadherin) and the "Plot Profile" function in FIJI was used to obtain a list of intensity values for each line. The intensity values were normalized to the highest pixel intensity measured in the experiment and plotted. Samples of inferior staining quality were eliminated from analysis. Staining and imaging conditions were kept consistent between samples.

Supernumerary polar cell load during oogenesis was scored by scanning through whole ovarioles and counting the number of polar cells present at each pole using FasIII and Eya as markers for polar cell fate. Nuclear STAT intensity at stages 7-8 was quantified by measuring

10XSTAT::GFP reporter intensity by drawing lines across three nuclei on either side of polar cells The mean GFP intensity of each line was normalized to the mean DAPI signal for each nuclear measurement. All measurements were then normalized to the highest relative GFP intensity value measured in the experiment.

Figures, graphs, and statistics

Images were processed in FIJI and figures were assembled using Affinity Photo (Serif, Nottingham, United Kingdom). Illustrations were designed in Affinity Photo. Graphs and statistical tests were performed using GraphPad Prism 7 or Prism 9 (GraphPad Software, San Diego, CA, USA). All statistical tests and significance levels are listed in the figure legends for the figures in which they appear and in Table 4.

Acknowledgements

We would like to thank Denise Montell, Michelle Starz-Gaiano, Nick Brown, and Hyung Don Ryoo, the Vienna *Drosophila* Resource Center (VDRC), the Bloomington *Drosophila* Stock Center (BDSC), and the Developmental Studies Hybridoma Bank (DSHB) at the University of Iowa for fly protocols, fly stocks, and antibodies. We also thank Gibson Hoefgen and Manuel Garcia for general project assistance and maintenance of *Drosophila* strains and Emily Burghardt, Rehan Khan, and Yujun Chen for helpful comments on the manuscript. We acknowledge the Confocal Core, funded by the Kansas State University (KSU) College of Veterinary Medicine, which provided use of the Zeiss LSM 880 confocal microscope. We thank the KSU Statistics Consulting Laboratory for statistics advice. This work was supported by the National Science Foundation (NSF 2027617) to J.A.M. and a KSU Johnson Cancer Research Center Graduate Student Summer Stipend Award to C.L.M. and J.A.M.

References

Abramson, J. and Anderson, G. (2017). Thymic Epithelial Cells. *Annu. Rev. Immunol.* **35**, 85–118.

Alégot, H., Pouchin, P., Bardot, O. and Mirouse, V. (2018). Jak-Stat pathway induces Drosophila follicle elongation by a gradient of apical contractility. *eLife* **7**, e32943.

Asha, H., de Ruiter, N., Wang, M. and Hariharan, I. (1999). The Rap1 GTPase functions as a regulator of morphogenesis invivo. *The EMBO Journal* **18**, 605–615.

Bach, E. A., Ekas, L. A., Ayala-Camargo, A., Flaherty, M. S., Lee, H., Perrimon, N. and Baeg, G.-H. (2007). GFP reporters detect the activation of the Drosophila JAK/STAT pathway in vivo. *Gene Expression Patterns* **7**, 323–331.

Bai, J. and Montell, D. (2002). Eyes Absent, a key repressor of polar cell fate during *Drosophila* oogenesis. *Development* **129**, 5377–5388.

Balaji, R., Weichselberger, V. and Classen, A.-K. (2019). Response of epithelial cell and tissue shape to external forces *in vivo*. *Development* dev.171256.

Baum, J. S., Arama, E., Steller, H. and McCall, K. (2007). The Drosophila caspases Strica and Dronc function redundantly in programmed cell death during oogenesis. *Cell Death Differ* **14**, 1508–1517.

Beccari, S., Teixeira, L. and Rørth, P. (2002). The JAK/STAT pathway is required for border cell migration during Drosophila oogenesis. *Mechanisms of Development* **111**, 115–123.

Besse, F. and Pret, A.-M. (2003). Apoptosis-mediated cell death within the ovarian polar cell lineage of *Drosophila melanogaster*. *Development* **130**, 1017–1027.

Blanpain, C. and Fuchs, E. (2009). Epidermal homeostasis: a balancing act of stem cells in the skin. *Nat Rev Mol Cell Biol* **10**, 207–217.

Boettner, B. and Van Aelst, L. (2007). The Rap GTPase Activator *Drosophila* PDZ-GEF Regulates Cell Shape in Epithelial Migration and Morphogenesis. *Mol Cell Biol* **27**, 7966–7980.

Boettner, B., Harjes, P., Ishimaru, S., Heke, M., Fan, H. Q., Qin, Y., Van Aelst, L. and Gaul, U. (2003). The AF-6 Homolog Canoe Acts as a Rap1 Effector During Dorsal Closure of the Drosophila Embryo. *Genetics* **165**, 159–169.

Bonello, T. T., Perez-Vale, K. Z., Sumigray, K. D. and Peifer, M. (2018). Rap1 acts via multiple mechanisms to position Canoe/Afadin and adherens junctions and mediate apical-basal polarity establishment. *Development* dev.157941.

Borensztejn, A., Boissoneau, E., Fernandez, G., Agnès, F. and Pret, A.-M. (2013). JAK/STAT autocontrol of ligand-producing cell number through apoptosis. *Development* **140**, 195–204.

Borensztejn, A., Mascaro, A. and Wharton, K. A. (2018). JAK/STAT signaling prevents excessive apoptosis to ensure maintenance of the interfollicular stalk critical for Drosophila oogenesis. *Developmental Biology* **438**, 1–9.

Bröer, S. (2008). Amino Acid Transport Across Mammalian Intestinal and Renal Epithelia. *Physiological Reviews* **88**, 249–286.

Buckley, C. E. and St Johnston, D. (2022). Apical–basal polarity and the control of epithelial form and function. *Nat Rev Mol Cell Biol* **23**, 559–577.

Cetera, M. and Horne-Badovinac, S. (2015). Round and round gets you somewhere: collective cell migration and planar polarity in elongating Drosophila egg chambers. *Current Opinion in Genetics & Development* **32**, 10–15.

Chang, Y.-C., Wu, J.-W., Hsieh, Y.-C., Huang, T.-H., Liao, Z.-M., Huang, Y.-S., Mondo, J. A., Montell, D. and Jang, A. C.-C. (2018). Rap1 Negatively Regulates the Hippo Pathway to Polarize Directional Protrusions in Collective Cell Migration. *Cell Reports* **22**, 2160–2175.

Choi, W., Harris, N. J., Sumigray, K. D. and Peifer, M. (2013). Rap1 and Canoe/afadin are essential for establishment of apical–basal polarity in the *Drosophila* embryo. *MBoC* **24**, 945–963.

Clem, R. J., Fechheimer, M. and Miller, L. K. (1991). Prevention of Apoptosis by a Baculovirus Gene During Infection of Insect Cells. *Science* **254**, 1388–1390.

Crest, J., Diz-Muñoz, A., Chen, D.-Y., Fletcher, D. A. and Bilder, D. (2017). Organ sculpting by patterned extracellular matrix stiffness. *eLife* **6**, e24958.

Deng, W.-M., Althauser, C. and Ruohola-Baker, H. (2001). Notch-Delta signaling induces a transition from mitotic cell cycle to endocycle in *Drosophila* follicle cells. *Development* **128**, 4737–4746.

Duhart, J. C., Parsons, T. T. and Raftery, L. A. (2017). The repertoire of epithelial morphogenesis on display: Progressive elaboration of Drosophila egg structure. *Mechanisms of Development* **148**, 18–39.

Duszyc, K., Gomez, G. A., Schroder, K., Sweet, M. J. and Yap, A. S. (2017). In life there is death: How epithelial tissue barriers are preserved despite the challenge of apoptosis. *Tissue Barriers* **5**, e1345353.

Fernandez-Gonzalez, R. and Peifer, M. (2022). Powering morphogenesis: multiscale challenges at the interface of cell adhesion and the cytoskeleton. *MBoC* **33**, pe4.

Gloerich, M. and Bos, J. L. (2011). Regulating Rap small G-proteins in time and space. *Trends in Cell Biology* **21**, 615–623.

Guillot, C. and Lecuit, T. (2013). Mechanics of Epithelial Tissue Homeostasis and Morphogenesis. *Science* **340**, 1185–1189.

Haigo, S. L. and Bilder, D. (2011). Global Tissue Revolutions in a Morphogenetic Movement Controlling Elongation. *Science* **331**, 1071–1074.

Haigo, S. L., Hildebrand, J. D., Harland, R. M. and Wallingford, J. B. (2003). Shroom Induces Apical Constriction and Is Required for Hingepoint Formation during Neural Tube Closure. *Current Biology* **13**, 2125–2137.

Harris, T. J. C. and Tepass, U. (2010). Adherens junctions: from molecules to morphogenesis. *Nat Rev Mol Cell Biol* **11**, 502–514.

Hay, B. A., Wolff, T. and Rubin, G. M. (1994). Expression of baculovirus P35 prevents cell death in Drosophila. *Development* **120**, 2121–2129.

Hay, B. A., Wassarman, D. A. and Rubin, G. M. (1995). Drosophila homologs of baculovirus inhibitor of apoptosis proteins function to block cell death. *Cell* **83**, 1253–1262.

Hinck, L. and Näthke, I. (2014). Changes in cell and tissue organization in cancer of the breast and colon. *Current Opinion in Cell Biology* **26**, 87–95.

Huang, J., Wu, S., Barrera, J., Matthews, K. and Pan, D. (2005). The Hippo Signaling Pathway Coordinately Regulates Cell Proliferation and Apoptosis by Inactivating Yorkie, the Drosophila Homolog of YAP. *Cell* **122**, 421–434.

Irvine, K. D. and Wieschaus, E. (1994). Cell intercalation during Drosophila germband extension and its regulation by pair-rule segmentation genes. *Development* **120**, 827–841.

Isabella, A. J. and Horne-Badovinac, S. (2016). Rab10-Mediated Secretion Synergizes with Tissue Movement to Build a Polarized Basement Membrane Architecture for Organ Morphogenesis. *Developmental Cell* **38**, 47–60.

Keller, R. E. (1981). An experimental analysis of the role of bottle cells and the deep marginal zone in gastrulation ofXenopus laevis. *J. Exp. Zool.* **216**, 81–101.

Khammari, A., Agnès, F., Gandille, P. and Pret, A.-M. (2011). Physiological apoptosis of polar cells during Drosophila oogenesis is mediated by Hid-dependent regulation of Diap1. *Cell Death Differ* **18**, 793–805.

Kim, Y. S., Fan, R., Lith, S. C., Dicke, A.-K., Drexler, H. C. A., Kremer, L., Kuempel-Rink, N., Hekking, L., Stehling, M. and Bedzhov, I. (2022). Rap1 controls epiblast morphogenesis in sync with the pluripotency states transition. *Developmental Cell* **57**, 1937-1956.e8.

Knox, A. L. and Brown, N. H. (2002). Rap1 GTPase Regulation of Adherens Junction Positioning and Cell Adhesion. *Science* **295**, 1285–1288.

Kuipers, D., Mehonic, A., Kajita, M., Peter, L., Fujita, Y., Duke, T., Charras, G. and Gale, J. E. (2014). Epithelial repair is a two-stage process driven first by dying cells and then by their neighbours. *Journal of Cell Science* jcs.138289.

Le, A. P., Rupprecht, J.-F., Mège, R.-M., Toyama, Y., Lim, C. T. and Ladoux, B. (2021). Adhesion-mediated heterogeneous actin organization governs apoptotic cell extrusion. *Nat Commun* **12**, 397.

Lebo, D. P. V. and McCall, K. (2021). Murder on the Ovarian Express: A Tale of Non-Autonomous Cell Death in the Drosophila Ovary. *Cells* **10**, 1454.

Lerner, D. W., McCoy, D., Isabella, A. J., Mahowald, A. P., Gerlach, G. F., Chaudhry, T. A. and Horne-Badovinac, S. (2013). A Rab10-Dependent Mechanism for Polarized Basement Membrane Secretion during Organ Morphogenesis. *Developmental Cell* **24**, 159–168.

Li, M., Sun, S., Priest, J., Bi, X. and Fan, Y. (2019). Characterization of TNF-induced cell death in Drosophila reveals caspase- and JNK-dependent necrosis and its role in tumor suppression. *Cell Death Dis* **10**, 613.

Loyer, N., Kolotuev, I., Pinot, M. and Le Borgne, R. (2015). *Drosophila* E-cadherin is required for the maintenance of ring canals anchoring to mechanically withstand tissue growth. *Proc. Natl. Acad. Sci. U.S.A.* **112**, 12717–12722.

Martin, A. C. and Goldstein, B. (2014). Apical constriction: themes and variations on a cellular mechanism driving morphogenesis. *Development* **141**, 1987–1998.

Martin, A. C., Kaschube, M. and Wieschaus, E. F. (2009). Pulsed contractions of an actin–myosin network drive apical constriction. *Nature* **457**, 495–499.

Munjal, A. and Lecuit, T. (2014). Actomyosin networks and tissue morphogenesis. *Development* **141**, 1789–1793.

Niewiadomska, P., Godt, D. and Tepass, U. (1999). DE-Cadherin Is Required for Intercellular Motility during Drosophila Oogenesis. *Journal of Cell Biology* **144**, 533–547.

Osswald, M., Barros-Carvalho, A., Carmo, A. M., Loyer, N., Gracio, P. C., Sunkel, C. E., Homem, C. C. F., Januschke, J. and Morais-de-Sá, E. (2022). aPKC regulates apical constriction to prevent tissue rupture in the Drosophila follicular epithelium. *Current Biology* S0960982222013859.

Paré, A. C. and Zallen, J. A. (2020). Cellular, molecular, and biophysical control of epithelial cell intercalation. In *Current Topics in Developmental Biology*, pp. 167–193. Elsevier.

Peifer, M., Orsulic, S., Sweeton, D. and Wieschaus, E. (1993). A role for the Drosophila segment polarity gene armadillo in cell adhesion and cytoskeletal integrity during oogenesis. *Development* **118**, 1191–1207.

Perez-Vale, K. Z. and Peifer, M. (2020). Orchestrating morphogenesis: building the body plan by cell shape changes and movements. *Development* **147**, dev191049.

Potla, U., Ni, J., Vadaparampil, J., Yang, G., Leventhal, J. S., Campbell, K. N., Chuang, P. Y., Morozov, A., He, J. C., D'Agati, V. D., et al. (2014). Podocyte-specific RAP1GAP expression contributes to focal segmental glomerulosclerosis–associated glomerular injury. *J. Clin. Invest.* **124**, 1757–1769.

Rodriguez-Boulan, E. and Macara, I. G. (2014). Organization and execution of the epithelial polarity programme. *Nat Rev Mol Cell Biol* **15**, 225–242.

Rosenblatt, J., Raff, M. C. and Cramer, L. P. (2001). An epithelial cell destined for apoptosis signals its neighbors to extrude it by an actin- and myosin-dependent mechanism. *Current Biology* **11**, 1847–1857.

Royou, A., Field, C., Sisson, J. C., Sullivan, W. and Karess, R. (2004). Reassessing the Role and Dynamics of Nonmuscle Myosin II during Furrow Formation in Early *Drosophila* Embryos. *MBoC* **15**, 838–850.

Ruohola, H., Bremer, K. A., Baker, D., Swedlow, J. R., Jan, L. Y. and Jan, Y. N. (1991). Role of neurogenic genes in establishment of follicle cell fate and oocyte polarity during oogenesis in Drosophila. *Cell* **66**, 433–449.

Sarpal, R., Pellikka, M., Patel, R. R., Hui, F. Y. W., Godt, D. and Tepass, U. (2012). Mutational analysis supports a core role for *Drosophila* α-Catenin in adherens junction function. *Journal of Cell Science* **125**, 233–245.

Sasaki, K., Kojitani, N., Hirose, H., Yoshihama, Y., Suzuki, H., Shimada, M., Takayanagi, A., Yamashita, A., Nakaya, M., Hirano, H., et al. (2020). Shank2 Binds to aPKC and Controls Tight Junction Formation with Rap1 Signaling during Establishment of Epithelial Cell Polarity. *Cell Reports* **31**, 107407.

Sawant, K., Chen, Y., Kotian, N., Preuss, K. M. and McDonald, J. A. (2018). Rap1 GTPase promotes coordinated collective cell migration in vivo. *MBoC* **29**, 2656–2673.

Sawyer, J. K., Harris, N. J., Slep, K. C., Gaul, U. and Peifer, M. (2009). The Drosophila afadin homologue Canoe regulates linkage of the actin cytoskeleton to adherens junctions during apical constriction. *Journal of Cell Biology* **186**, 57–73.

Silver, D. L. and Montell, D. J. (2001). Paracrine Signaling through the JAK/STAT Pathway Activates Invasive Behavior of Ovarian Epithelial Cells in Drosophila. *Cell* **107**, 831–841.

Spahn, P., Ott, A. and Reuter, R. (2012). The PDZ-GEF Dizzy regulates the establishment of adherens junctions required for ventral furrow formation in *Drosophila*. *Journal of Cell Science* jcs.101196.

Spradling A. C. (1993). Developmental genetics of oogenesis. In *The Development of Drosophila Melanogaster*, pp. 1-70. CSHL Press.

Tai, K., Cockburn, K. and Greco, V. (2019). Flexibility sustains epithelial tissue homeostasis. *Current Opinion in Cell Biology* **60**, 84–91.

Uechi, H. and Kuranaga, E. (2018). Mechanisms of unusual collective cell movement lacking a free front edge in Drosophila. *Current Opinion in Genetics & Development* **51**, 46–51.

Wang, Y.-C., Khan, Z. and Wieschaus, E. F. (2013). Distinct Rap1 Activity States Control the Extent of Epithelial Invagination via α-Catenin. *Developmental Cell* **25**, 299–309.

Wang, A., Dunn, A. R. and Weis, W. I. (2022). Mechanism of the cadherin–catenin F-actin catch bond interaction. *eLife* **11**, e80130.

Williams-Masson, E. M., Malik, A. N. and Hardin, J. (1997). An actin-mediated two-step mechanism is required for ventral enclosure of the C. elegans hypodermis. *Development* **124**, 2889–2901.

Wu, S., Huang, J., Dong, J. and Pan, D. (2003). hippo Encodes a Ste-20 Family Protein Kinase that Restricts Cell Proliferation and Promotes Apoptosis in Conjunction with salvador and warts. *Cell* **114**, 445–456.

Yan, N., Wu, J.-W., Chai, J., Li, W. and Shi, Y. (2004). Molecular mechanisms of DrICE inhibition by DIAP1 and removal of inhibition by Reaper, Hid and Grim. *Nat Struct Mol Biol* **11**, 420–428.

Yonemura, S., Wada, Y., Watanabe, T., Nagafuchi, A. and Shibata, M. (2010). α-Catenin as a tension transducer that induces adherens junction development. *Nat Cell Biol* **12**, 533–542.

Zajac, A. L. and Horne-Badovinac, S. (2022). Kinesin-directed secretion of basement membrane proteins to a subdomain of the basolateral surface in Drosophila epithelial cells. *Current Biology* **32**, 735-748.e10.

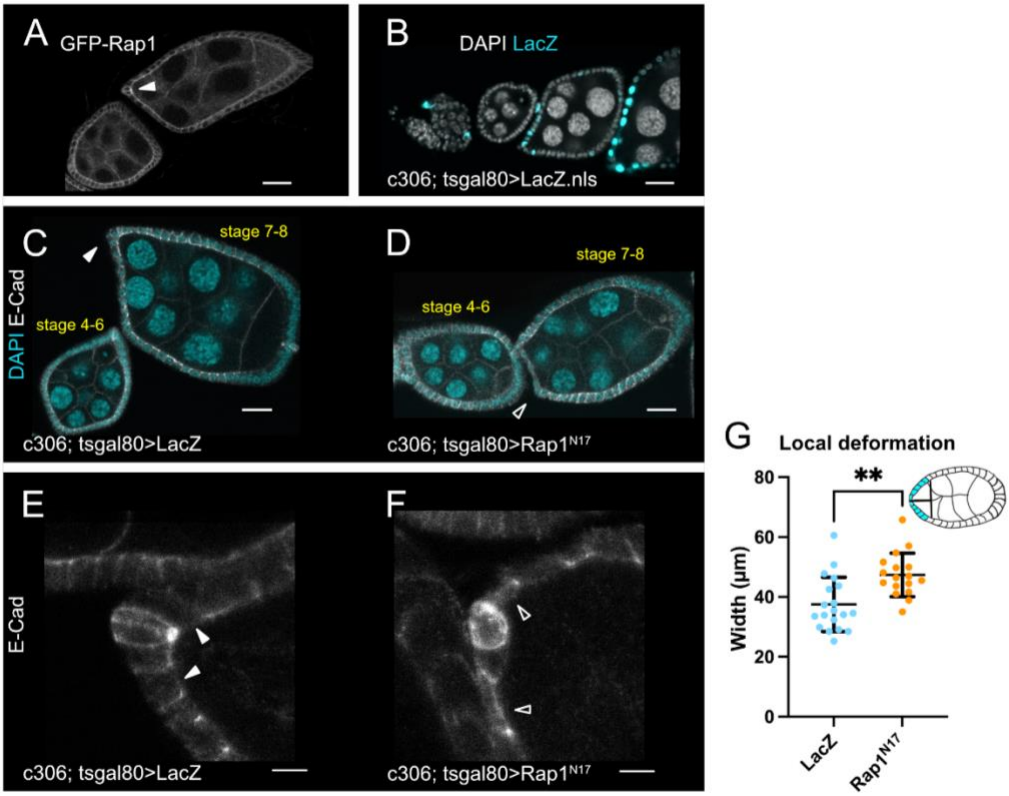

Figure 1. Rap1 is required in the anterior epithelium to maintain follicle cell and egg chamber shape

(A) Ovariole with GFP tagged Rap1 illustrates Rap1 enrichment in follicle cells. Arrowhead indicates apical Rap1 accumulation in anterior epithelium. (B) Ovariole expressing UAS-LacZ driven by *c306*-GAL4 to demonstrate the *c306*-GAL4 expression pattern. (C-D) LacZ control (C) or DN-Rap1^{N17} (D) egg chambers. Anterior epithelia are distorted at stages 7-8 in DN-Rap1^{N17}. Arrowheads indicate anterior region of stage 7-8 egg chambers. Solid arrowhead points to normal anterior epithelium of control (C), while open arrowhead indicates distorted anterior region for DN-Rap1^{N17} (D). (E-F) Anterior regions of stage 7-8 egg chambers showing normal cuboidal epithelium in control (E) or stretched cell shapes in DN-Rap1^{N17} (F). Solid arrowheads indicate cuboidal shaped cells in E. Open arrowheads indicate stretched cells in F. (G) Quantification of local deformation measures taken at 20% of egg chamber length (illustrated by egg chamber schematic in G). ** $p \leq 0.01$ two-tailed unpaired t-test. $N \geq 17$ egg chambers measured per genotype. (A-D) Scale bars 20µm. (E-F) Scale bars 5µm.

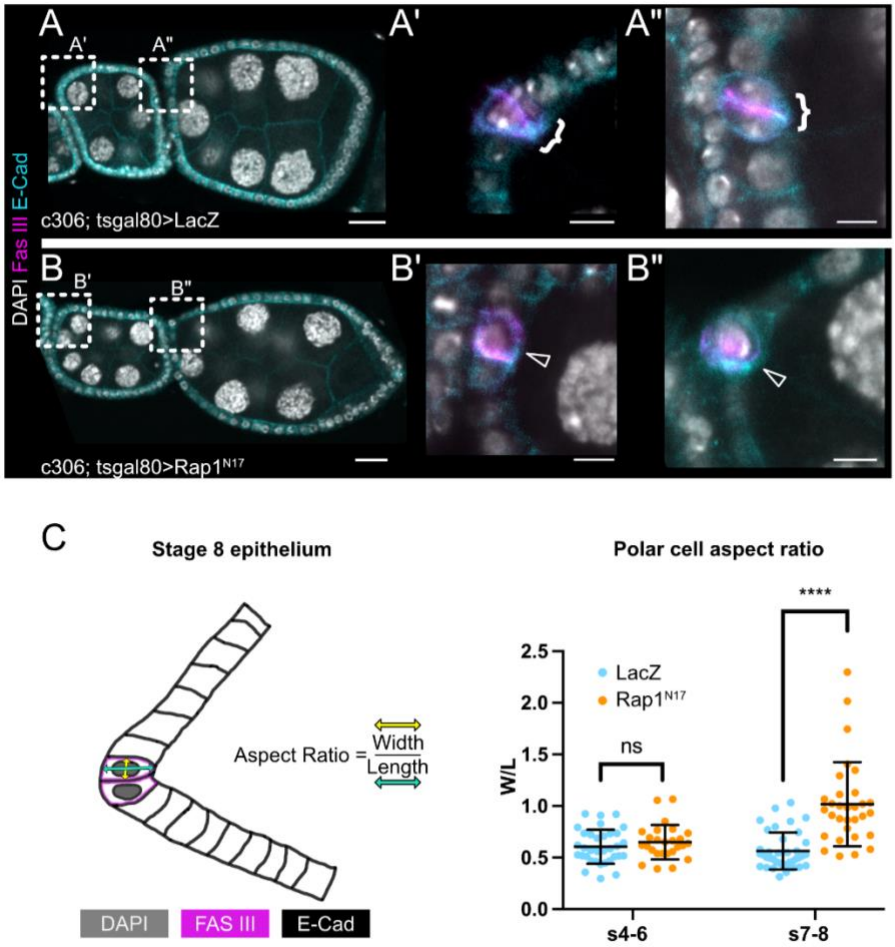

Figure 2. Rap1 is required for proper polar cell shape

(A-B) LacZ (A) and DN-Rap1^{N17} (B) ovarioles imaged for polar cell shape. Dashed boxes indicate the regions expanded in A', A", B', and B". (A'-A", B'-B") Close-up views of anterior egg chamber regions. Control stage 4-6 (A') and stage 7-8 (A") egg chamber polar cells. Brackets indicate intact polar cell pairs. (B'-B") DN-Rap1^{N17} stage 4-6 (B') and stage 7-8 (B") egg chamber polar cells. (B') Only one polar cell is present at stage 4-6. (B") One spherical polar cell is present at stage 7-8. Open arrowheads indicate only one polar cell is present. (C) Aspect ratio schematic and quantification. Aspect ratio (AR) was defined as the dorsoventral (DV) width divided by the anterior-posterior (AP) length. AR measurements plotted for stage 4-6 and stage 7-8 egg chamber polar cells. DN-Rap1^{N17} polar cells are more spherical at stage 7-8 indicated by average AR=1.02 vs average AR=0.56 for control. **** $p \leq 0.0001$ two-tailed unpaired t test. N≥26 polar cells measured per genotype per egg chamber stage. (A-B) Scale bars 20μm. (A'-B") Scale bars 5μm.

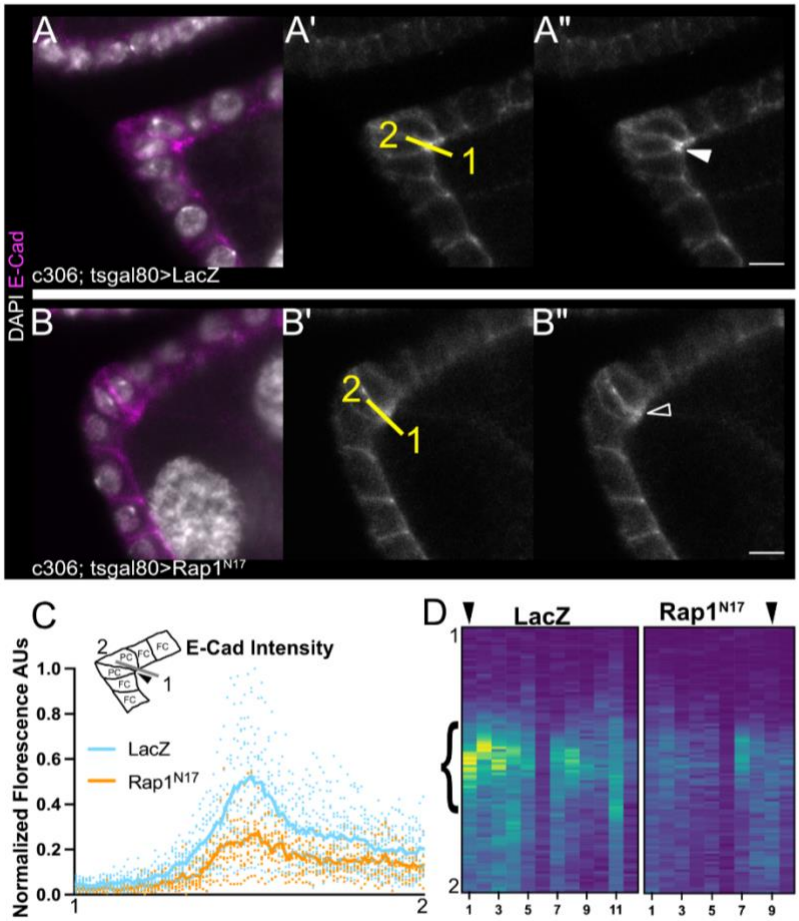

Figure 3. Rap1 is required for apical E-Cadherin enrichment in polar cells

(A-B) Anterior regions of stage 7-8 egg chambers for LacZ control (A) and DN-Rap1^{N17} egg chambers (B). (A'-B") Single channel panels of A and B showing E-Cadherin (gray) enrichment. (A', B') Yellow line indicates region of measurement beginning over nurse cells (1) and ending along lateral polar cell-polar cell interface (2). Solid arrowhead indicates apical accumulation of E-Cadherin. Open arrowhead indicates reduced E-Cadherin enrichment. (A", B") Same as A' and B' without line overlays for clarity. Image brightness adjusted for presentation purposes. (C) Measurement schematic and quantification of fluorescence intensities measured along lines drawn as in A' and B' and normalized to highest signal. Lines represent mean intensity. (D) Heat map representation of C. Bracket indicates area of heat map corresponding to apical enrichment of E-Cadherin in polar cells. Arrowheads at the top of heat map indicate the lanes corresponding to A" and B". Scale bars 5µm.

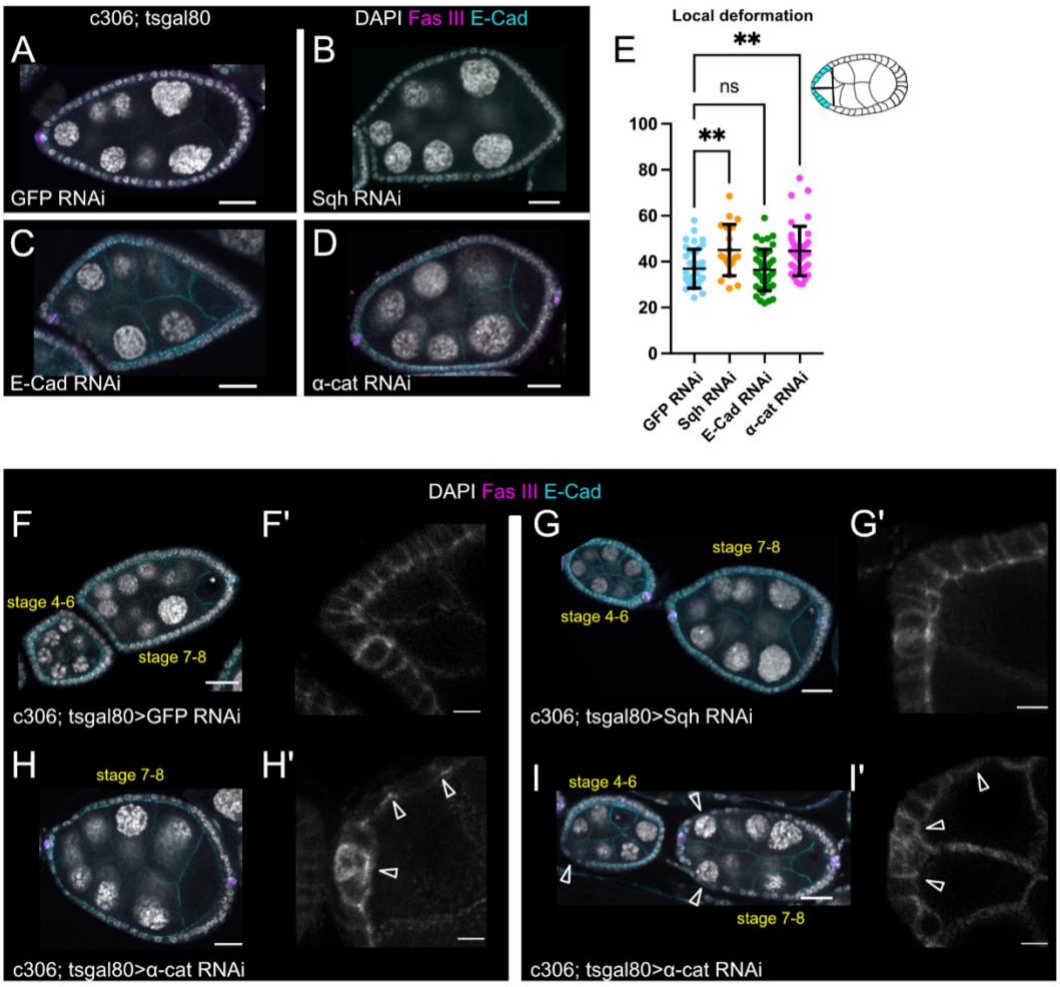

Figure 4. Sqh and α-Catenin maintain local tissue shape and α-Catenin is also required for epithelial integrity

(A-D) Stage 7-8 GFP RNAi (A), Sqh RNAi, (B) E-Cadherin RNAi (C), and α-cat RNAi (D) egg chambers imaged for egg chamber shape. (E) Schematic and quantification of local deformation measurement. ** p≤0.01 One-way ANOVA followed by Dunnett's multiple comparisons test. N≥19 egg chambers per genotype. (F-I) GFP RNAi (F), Sqh RNAi (G), and α-cat RNAi (H-I) ovarioles imaged to show egg chamber shape and anterior epithelium. (F'-I') Maximum intensity projections of anterior regions of stage 7-8 egg chambers pictured in the main panels. Open arrowheads in H', I, and I' indicate "stretched" or clustered cells observed in α-cat RNAi egg chambers. (A-D, F-I) Scale bars 20μm. (F'-I') Scale bars 5μm.

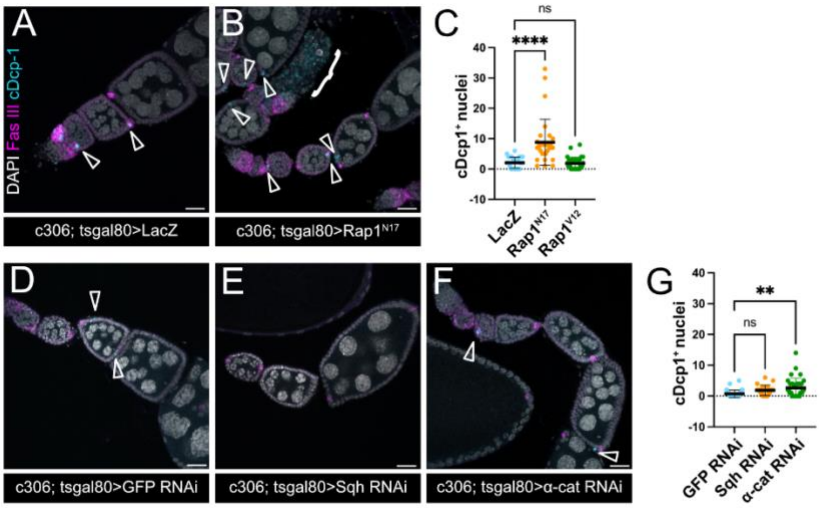

Figure 5. Rap1 and α-Catenin are required for cell viability during oogenesis

(A-B) Maximum intensity projections of ovarioles showing caspase positive nuclei for LacZ (A) and DN-Rap1^{N17} (B). Open arrowheadss in A and B indicate cDcp1 positive nuclei and the bracket in B indicates a degenerating egg chamber. (C) Quantification of cDcp1 positive nuclei per ovariole (egg chamber stages 2-8 only). DN-Rap1^{N17} ovarioles have greater number of cDcp1 positive nuclei. **** p≤0.0001 One-way ANOVA followed by Dunnett's multiple comparisons test. N≥29 ovarioles per genotype. (D-F) Maximum intensity projections of ovarioles for GFP RNAi (D), Sqh RNAi (E), and α-cat RNAi (F). Open arrowheads indicate cDcp1 positive nuclei. (G) Quantification of cDcp1 positive nuclei. ** p≤0.01 One-way ANOVA followed by Dunnett's multiple comparisons test. N≥20 ovarioles per genotype. Scale bars 20µm.

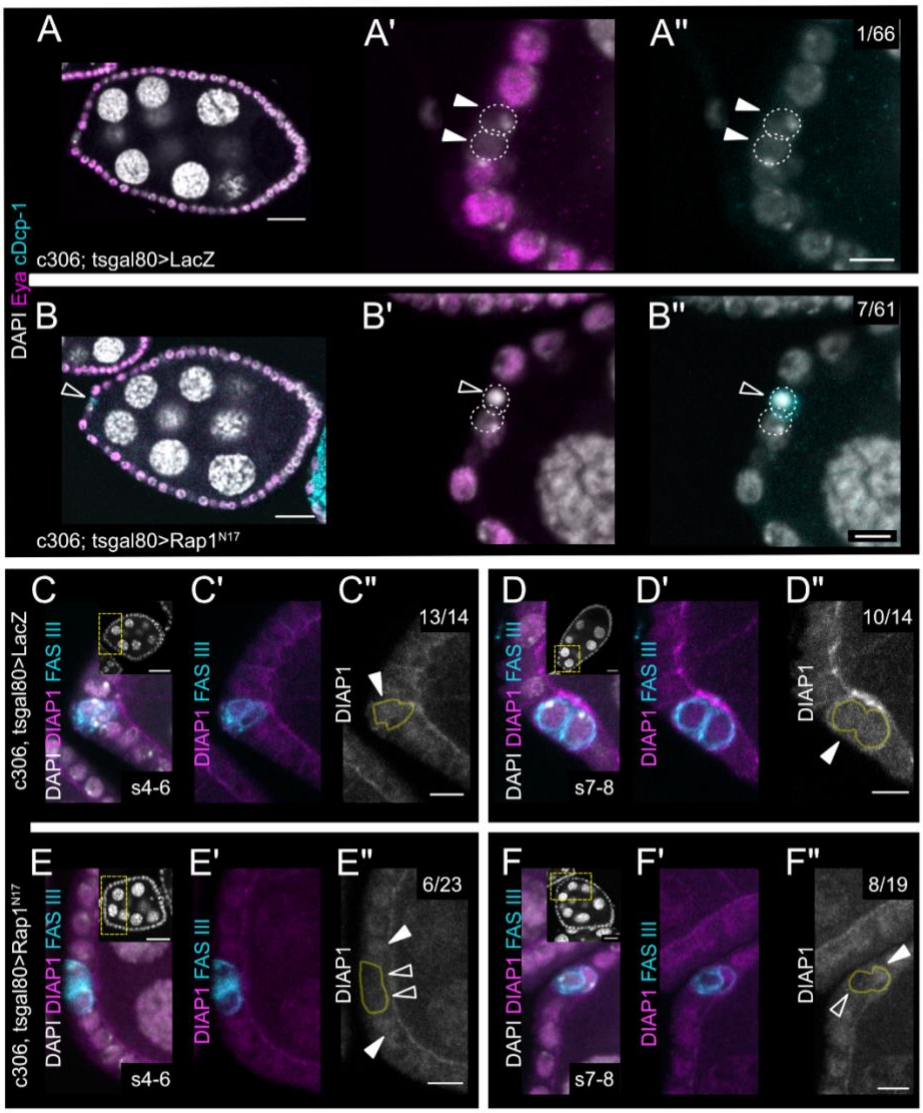

Figure 6. Rap1 is required for polar cell viability and proper DIAP1 accumulation

(A-B) Stage 7-8 LacZ (A) and DN-Rap1^{N17} (B) egg chambers scored for cDcp1 positive polar cells . (A', B') Close-up views of anterior regions of the egg chambers depicted in A and B, showing only DAPI and Eya staining. (A", B") Same images as A' and B' showing only DAPI and cDcp1. Filled arrowheads in A' and A" indicate viable mature polar cells. Open arrowheads in B' and B" indicate a cDcp1 positive dying polar cell. Numbers in A" and B" indicate number of observations of cDcp1 positive polar cells per stage 7-8 egg chambers scored. (C-C", E-E") Stage 4-6 LacZ (C-C") and DN-Rap1^{N17} (E-E") egg chambers. (C', E') Same images as C and E showing only DIAP1 and FasIII. (C", E") DIAP1 only. (D-D", F-F") Stage 7-8 LacZ (D-D") and DN-Rap1^{N17} (F-F") egg chambers. (C-F) Insets show DAPI-stained whole egg chambers corresponding to zoomed regions with yellow boxes outlining the approximate region depicted in main panels. (C"-F") Polar cells are outlined in yellow. Solid arrowheads indicate normal DIAP1

accumulation. Open arrowheads indicate reduced DIAP1. The number of egg chambers with normal DIAP1 accumulation out of total egg chambers scored is reported in the upper right of C”, D”, E”, and F”. (A-F) Scale bars 20μm. (C”-F”) Scale bars 5μm.

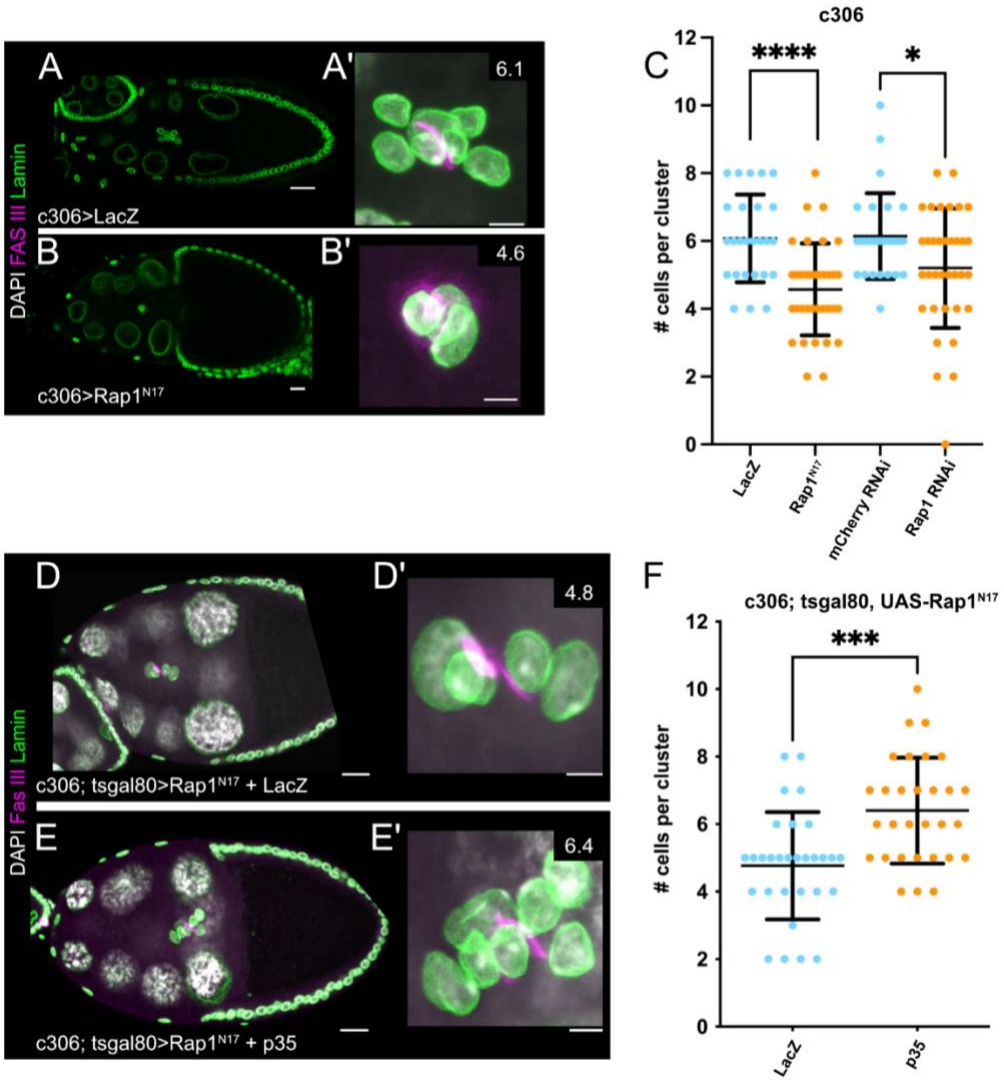

Figure 7. Rap1 dependent cell viability is required for proper border cell cluster assembly (A-B) Stage 9-10 egg chambers for LacZ (A) and DN-Rap1^{N17} (B). (A'-B') Maximum intensity projections of border cell clusters from egg chambers pictured in A and B. Numbers at top right are average number of cells observed for each genotype. (C) Quantification of cell number per cluster for each genotype. * $p \leq 0.05$ ****$p \leq 0.0001$ two-tailed unpaired t test. N≥26 border cell clusters per genotype. (D-E) Stage 9-10 egg chambers for DN-Rap1^{N17} + LacZ expression control (D) or DN-Rap1^{N17} + p35 (E). (D'- E') Maximum intensity projections of border cell clusters from egg chambers pictured in D and E. Numbers at top right are average number of cells observed for each genotype. (F) Quantification of cell number per cluster for each genotype. *** $p \leq 0.001$ two-tailed unpaired t test. N=30 border cell clusters per genotype. (A-B, D-E) Scale bars 20μm. (A'-B', D'-E') Scale bars 5μm.

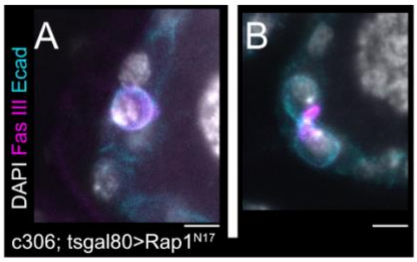

Figure S1. Rap1 inhibition causes polar cell loss and distorted polar cell shapes

(A-B) Anterior regions of two different DN-Rap1^{N17} stage 7-8 egg chambers. (A) Only one mature polar cell is present. (B) A pair of polar cells stretched along the dorsoventral axis. Scale bars 5µm.

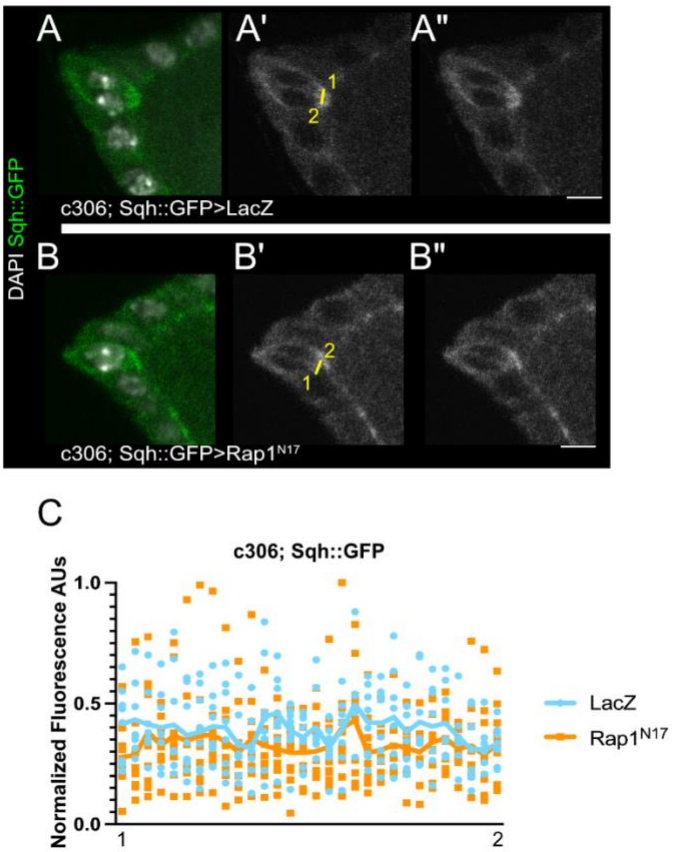

Figure S2. Rap1 is dispensable for Sqh apical localization in polar cells

(A-B) Anterior regions of stage 7-8 egg chambers for LacZ (A) or DN-Rap1^{N17} (B). (A'-B') Single channel images of A and B showing GFP (gray) with yellow lines indicating region of measurement for Sqh::GFP intensity. The numbers correspond to the plot intensity profiles in C. (A"-B") Single channel images as in A' and B' with line removed for clarity. The image brightness was adjusted for presentation purposes but not used for quantification. (C) Profile of the intensity values along the measurement lines, plotted and normalized to highest signal. The numbers on the x-axis correspond to the lines drawn on A' and B'. Solid plot lines represent the mean intensity. N ≥ 8 egg chambers per genotype. Scale bars 5µm.

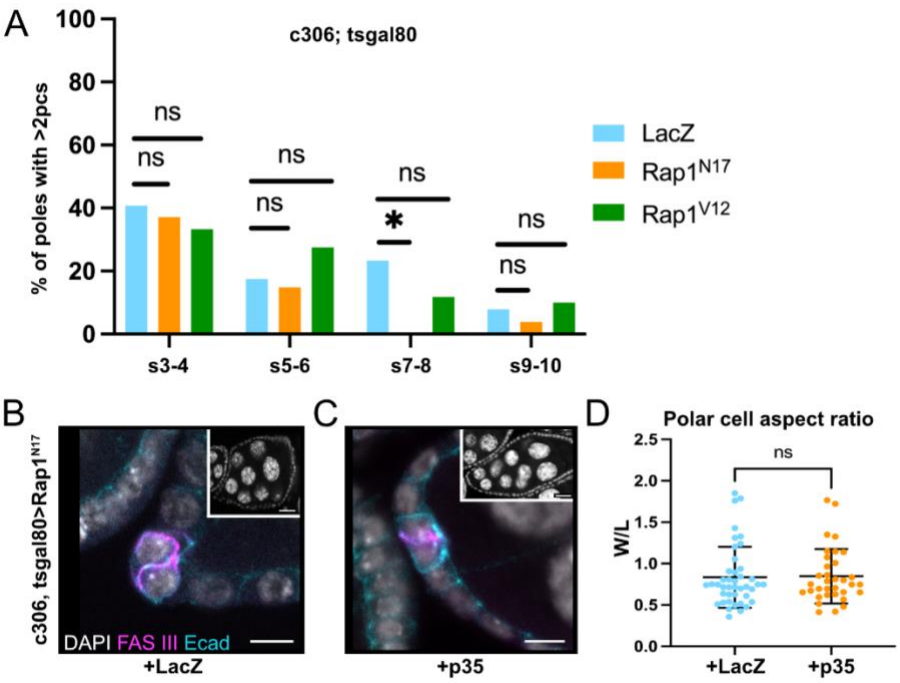

Figure S3. Rap1 does not regulate early elimination of supernumerary polar cells and maintains mature polar cell shape independent of apoptosis

(A) Quantification showing frequency of egg chamber poles with supernumerary polar cells during specific stages of oogenesis. * $p \leq 0.05$ two-sided Fisher's exact test. N≥30 egg chamber poles per stage per genotype. Supernumerary polar cells are present early for all genotypes. (B-C) Anterior region of stage 7-8 egg chambers, DN-Rap1^{N17} with LacZ expression (A) or DN-Rap1^{N17} with apoptosis inhibitor p35 (B). Whole egg chambers stained for DAPI are shown in the insets. (D) Polar cell aspect ratio quantification. Mean AR of DN-Rap1^{N17} + LacZ control = 0.84. Mean AR of DN-Rap1^{N17} + p35 = 0.85. NS two-tailed unpaired t test. N≥34 polar cells per genotype. Main panel scale bars 5µm. Inset scale bars 20µm.

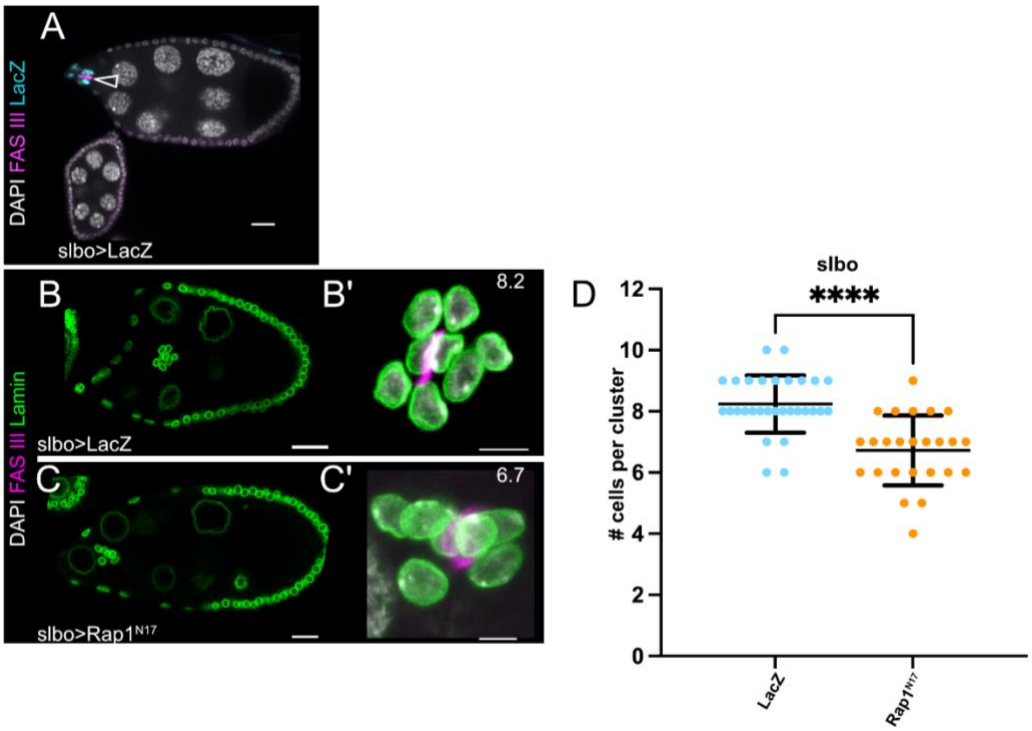

Figure S4. Effects of late Rap1 inhibition on border cell numbers

(A) Ovariole region expressing UAS-LacZ indicates the expression pattern of *slbo*-GAL4. (B-C) Stage 9-10 LacZ (B) and DN-Rap1^{N17} (C) egg chambers showing mid-migration border cells. (B'-C') Maximum intensity projections of border cell clusters from B and C. Numbers in the upper right indicate the average number of cells per cluster. (D) Quantification of cell number per cluster for Rap1 inhibition using *slbo*-GAL4. **** $p \leq 0.0001$ two-tailed unpaired t test. $N \geq 25$ border cell clusters per genotype. (A-C) Scale bars 20μm. (B'-C') Scale bars 5μm.

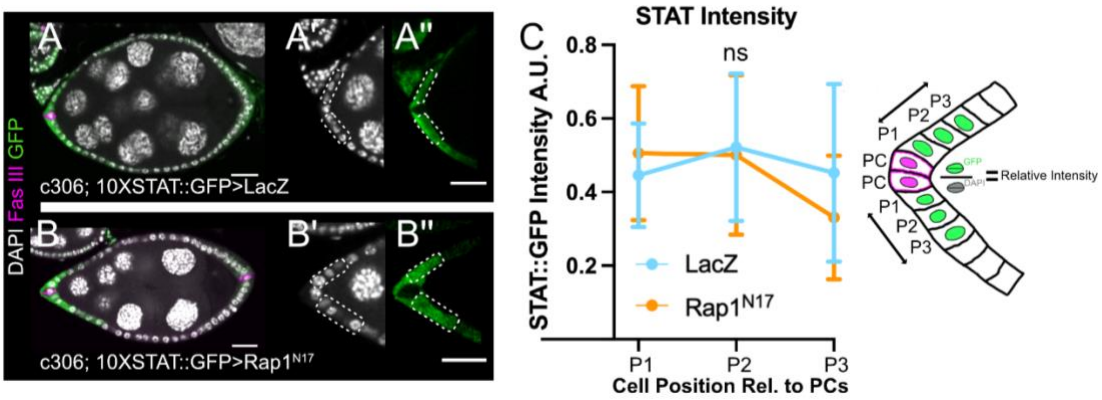

Figure S5. Rap1 is dispensable for STAT levels in follicle cells fated to become border cells

(A, B) Stage 8 LacZ (A) and DN-Rap1^{N17} (B) egg chambers with 10XSTAT::GFP reporter expression enriched adjacent to anterior polar cells. (A'-A", B'-B") Insets of the anterior end of the egg chambers in A and B, which was used to measure the intensity of nuclear 10XSTAT::GFP. (A'-B') DAPI. (A"-B") 10XSTAT::GFP. Dashed rectangles indicate the cell positions next to polar cells used for analyzing STAT levels. (C) Schematic and plot of STAT intensity values relative to the DAPI signal and normalized to the highest intensity STAT measurement. NS, unpaired two-tailed t-test. N≥12 follicle cells at each position pooled from N≥6 stage 8 egg chambers for each genotype. (A-B) Scale bars 20μm. (A"-B") Scale bars 5μm.

Table 1. Fly strains used in this study.

Fly Stock	Source	Appears in Figures
c306-GAL4		7
c306-GAL4; 10XSTAT92E-GFP	M. Starz-Gaiano	S5
c306-GAL4; UAS-Rap1N17, tsgal80	This study	7, S3
c306-GAL4; Sqh::GFP	P. Majumder	S2
c306-GAL4; tsgal80	P. Majumder	1, 2, 3, 4, 5, 6, S1, S3
c306-GAL4, tsgal80; PT Fas III (GFP)	This study	6
slbo-GAL4	BDSC 58435	S4
GFP-Rap1	N. Brown	1
UAS-α-Catenin RNAi	VDRC v107298	4, 5
UAS-E-Cadherin RNAi	VDRC v103962	4
UAS-GFP RNAi	VDRC v60102	4, 5
UAS-LacZ.nls	D. Montell	1, 2, 3, 5, 6, 7, S2, S3, S4, S5
UAS-mCherry RNAi	BDSC 35785	7
UAS-p35.H	BDSC 5072	7, S3
UAS-Rap1N17	B. Boettner	1, 2, 3, 5, 6, 7, S1, S2, S3, S4, S5
UAS-Rap1 RNAi	VDRC v33437	7
UAS-Rap1V12	B. Boettner	5, S3
UAS-Sqh RNAi	VDRC v7916	4, 5

Table 2. Genotypes in this study.

Figure	Genotypes
1A	w; P[w+ GFP-Rap1]
1B	c306-GAL4/w; tsgal80/+; UAS-LacZ.nls/+
1C	c306-GAL4/w; tsgal80/+; UAS-LacZ.nls/+
1D	c306-GAL4/w; tsgal80/UAS-Rap1N17; TM2/+
1E	c306-GAL4/w; tsgal80/+; UAS-LacZ.nls/+
1F	c306-GAL4/w; tsgal80/UAS-Rap1N17; TM2/+
1G	c306-GAL4/w; tsgal80/+; UAS-LacZ.nls/+ c306-GAL4/w; tsgal80/UAS-Rap1N17; TM2/+
2A-A"	c306-GAL4/w; tsgal80/+; UAS-LacZ.nls/+
2B-B"	c306-GAL4/w; tsgal80/UAS-Rap1N17; TM2/+
2C	c306-GAL4/w; tsgal80/+; UAS-LacZ.nls/+ c306-GAL4/w; tsgal80/UAS-Rap1N17; TM2/+
3A-A"	c306-GAL4/w; tsgal80/+; UAS-LacZ.nls/+
3B-B"	c306-GAL4/w; tsgal80/UAS-Rap1N17; TM2/+
3C-D	c306-GAL4/w; tsgal80/+; UAS-LacZ.nls/+ c306-GAL4/w; tsgal80/UAS-Rap1N17; TM2/+
4A	c306-GAL4/w; tsgal80/UAS-GFP-RNAi
4B	c306-GAL4/w; tsgal80/UAS-Sqh-RNAi
4C	c306-GAL4/w; tsgal80/UAS-E-Cadherin-RNAi
4D	c306-GAL4/w; tsgal80/UAS-α-Catenin-RNAi
4E	c306-GAL4/w; tsgal80/UAS-GFP-RNAi c306-GAL4/w; tsgal80/UAS-Sqh-RNAi c306-GAL4/w; tsgal80/UAS-E-Cadherin-RNAi c306-GAL4/w; tsgal80/UAS-α-Catenin-RNAi
4F-F'	c306-GAL4/w; tsgal80/UAS-GFP-RNAi
4G-G'	c306-GAL4/w; tsgal80/UAS-Sqh-RNAi
4H-H'	c306-GAL4/w; tsgal80/UAS-α-Catenin-RNAi
4I-I'	c306-GAL4/w; tsgal80/UAS-α-Catenin-RNAi
5A	c306-GAL4/w; tsgal80/+; UAS-LacZ.nls/+
5B	c306-GAL4/w; tsgal80/UAS-Rap1N17; TM2/+
5C	c306-GAL4/w; tsgal80/+; UAS-LacZ.nls/+ c306-GAL4/w; tsgal80/UAS-Rap1N17; TM2/+ c306-GAL4/w; tsgal80/BL; UAS-Rap1V12/+
5D	c306-GAL4/w; tsgal80/UAS-GFP-RNAi
5E	c306-GAL4/w; tsgal80/UAS-Sqh-RNAi
5F	c306-GAL4/w; tsgal80/UAS-α-Catenin-RNAi
5G	c306-GAL4/w; tsgal80/UAS-GFP-RNAi c306-GAL4/w; tsgal80/UAS-Sqh-RNAi c306-GAL4/w; tsgal80/UAS-α-Catenin-RNAi
6A-A"	c306-GAL4/w; tsgal80/+; UAS-LacZ.nls/+
6B-B"	c306-GAL4/w; tsgal80/UAS-Rap1N17; TM2/+
6C-C"	c306-GAL4, tsgal80/w; PT Fas III (GFP)/+; UAS-LacZ.nls/+
6D-D"	c306-GAL4, tsgal80/w; PT Fas III (GFP)/+; UAS-LacZ.nls/+
6E-E"	c306-GAL4, tsgal80/w; PT Fas III (GFP)/UAS-Rap1N17; TM2/+
6F-F"	c306-GAL4, tsgal80/w; PT Fas III (GFP)/UAS-Rap1N17; TM2/+

7A-A'	c306-GAL4/w; G13, L[2]/+; UAS-LacZ.nls/+
7B-B'	c306-GAL4/w; G13, L[2]/UAS-Rap1N17; TM2/+
7C	c306-GAL4/w; G13, L[2]/+; UAS-LacZ.nls/+ c306-GAL4/w; G13, L[2]/UAS-Rap1N17; TM2/+ c306-GAL4/w; G13, L[2]/+; UAS-mCherry-RNAi/+ c306-GAL4/w; G13, L[2]/+; UAS-Rap1-RNAi/+
7D-D'	c306-GAL4/w; tsgal80, UAS-Rap1N17/+; UAS-LacZ.nls/+
7E-E'	c306-GAL4/w; tsgal80, UAS-Rap1N17/UAS-p35.H
7F	c306-GAL4/w; tsgal80, UAS-Rap1N17/+; UAS-LacZ.nls/+ c306-GAL4/w; tsgal80, UAS-Rap1N17/UAS-p35.H
S1A-B	c306-GAL4/w; tsgal80/UAS-Rap1N17; TM2/+
S2A-A"	c306-GAL4/w; Sgh::GFP/+; UAS-LacZ.nls/+
S2B-B"	c306-GAL4/w; Sqh::GFP/UAS-Rap1N17; TM2/+
S2C	c306-GAL4/w; Sqh::GFP/+; UAS-LacZ.nls/+ c306-GAL4/w; Sqh::GFP/UAS-Rap1N17; TM2/+
S3A	c306-GAL4/w; tsgal80/+; UAS-LacZ.nls/+ c306-GAL4/w; tsgal80/UAS-Rap1N17; TM2/+ c306-GAL4/w; tsgal80/BL; UAS-Rap1V12/+
S3B	c306-GAL4/w; tsgal80, UAS-Rap1N17/+; UAS-LacZ.nls/+
S3C	c306-GAL4/w; tsgal80, UAS-Rap1N17/UAS-p35.H
S3D	c306-GAL4/w; tsgal80, UAS-Rap1N17/+; UAS-LacZ.nls/+ c306-GAL4/w; tsgal80, UAS-Rap1N17/UAS-p35.H
S4A	w; slbo-GAL4/UAS-LacZ.nls
S4B-B'	w; slbo-GAL4/UAS-LacZ.nls
S4C-C'	w; UAS-Rap1N17/+; slbo-GAL4/TM2
S4D	w; slbo-GAL4/UAS-LacZ.nls w; UAS-Rap1N17/+; slbo-GAL4/TM2
S5A-A"	c306-GAL4/w; 10XSTAT92E-GFP/+; UAS-LacZ.nls/+
S5B-B"	c306-GAL4/w; 10XSTAT92E-GFP/UAS-Rap1N17; TM2/+
S5C	c306-GAL4/w; 10XSTAT92E-GFP/+; UAS-LacZ.nls/+ c306-GAL4/w; 10XSTAT92E-GFP/UAS-Rap1N17; TM2/+

Table 3. Antibodies used in this study.

Antibody	Concentration	Source	Appears in Figures
Dcp-1 (Asp215)	(1:50-1:100)	Cell Signaling Technology	5, 6
DE-cadherin (DCAD2)	(1:10)	DSHB	1, 2, 3, 4, S1, S3
DIAP1	(1:100)	H. D. Ryoo	6
Eya (10H6)	(1:50-1:100)	DSHB	6
Fas3 (7G10)	(1:5-1:10)	DSHB	2, 4, 5, 7, S1, S3, S4, S5
GFP (12E6)	(1:10)	DSHB	1, S2
GFP (ab13970)	(1:100)	abcam	6, S5
LacZ (40-1a)	(1:10)	DSHB	1, S4
Lamin (ADL67.10)	(1:10)	DSHB	7, S4

Secondary antibodies used at a concentration of 1:400
Alexa Fluor Chicken 488 IgG H+L
Alexa Fluor Mouse 488 IgG H+L
Alexa Fluor Mouse 488 IgG1
Alexa Fluor Mouse 568 IgG H+L
Alexa Fluor Mouse 568 IgG2a
Alexa Fluor Rabbit 647 IgG H+L
Alexa Fluor Rat 488 IgG H+L
Alexa Fluor Rat 647 IgG H+L
DAPI (Millipore Sigma) was used at 0.05 µg/ml

Table 4. Statistics in this study.

Figure	Experimental Unit	Measurement	Experiments per Genotype (n)	Statistical Test	Significance
1G	Egg chamber	Anterior width	≥17	Unpaired two-tailed t test	**
2C	Polar cell	Aspect ratio	≥26	Unpaired two-tailed t test	ns, ****
3C	Egg chamber	Apical E-Cad Intensity	≥10	N/A	N/A
4E	Egg chamber	Anterior width	≥19	One-way ANOVA with Dunnett's Multiple Comparisons test	ns, **
5C	Ovariole	cDcp+ nuclei	≥29	One-way ANOVA with Dunnett's Multiple Comparisons test	ns, ****
5G	Ovariole	cDcp+ nuclei	≥20	One-way ANOVA with Dunnett's Multiple Comparisons test	ns, **
7C	Border cell clusters	Cells per cluster	≥26	Unpaired two-tailed t test	*, ****
7F	Border cell clusters	Cells per cluster	30	Unpaired two-tailed t test	***
S2C	Egg chamber	Apical Sqh Intensity	≥8	N/A	N/A
S3A	Egg chamber pole	Supernumerary polar cells	≥30	Fisher's exact test	ns, *
S3D	Polar cell	Aspect ratio	≥34	Unpaired two-tailed t test	ns
S4D	Border cell clusters	Cells per cluster	≥25	Unpaired two-tailed t test	****
S5C	Nucleus	Stat reporter intensity	≥12	Unpaired two-tailed t test	ns

Significance values: * P≤0.05, ** P≤0.01, ***P≤0.001, ****P<0.0001.